



41 **Abstract**

42 The ForestScan project was conceived to evaluate new technologies for characterising forest structure and biomass at Forest  
43 Biomass Reference Measurement Sites (FBRMS). It is closely aligned with other international initiatives, particularly the  
44 Committee on Earth Observation Satellites (CEOS) Working Group on Calibration & Validation (WGCV) [aboveground](#)  
45 [biomass \(AGB\)](#) cal/val protocols, and is part of GEO-TREES, an international consortium dedicated to establishing a global  
46 network of Forest Biomass Reference Measurement Sites (FBRMS) to support EO and encourage investment in relevant field-  
47 based observations and science. ForestScan is the first demonstration of what can be achieved more broadly under GEO-  
48 TREES, which would significantly expand and enhance the use of EO-derived AGB estimates.  
49

50 We present data from the ForestScan project, a unique multiscale dataset of tropical forest [three-dimensional \(3D\)](#) structural  
51 measurements, including terrestrial [laser](#) scanning (TLS), unpiloted aerial vehicle [laser](#) scanning (UAV-LS), airborne [laser](#)  
52 scanning (ALS), and in-situ tree census and ancillary data. These data are critical for the calibration and validation of [EO](#)  
53 estimates of forest biomass, as well as providing broader insights into tropical forest structure.  
54

**Deleted:** LiDAR

**Deleted:** LiDAR

**Deleted:** LiDAR

**Deleted:** earth observation (

**Deleted:** )

55 Data are presented for three FBRMS: FBRMS-01: Paracou, French Guiana; FBRMS-02: Lopé, Gabon; and FBRMS-03:  
56 Kibili-Sepilok, Malaysia. Field data for each site include new 3D LiDAR measurements combined with plot tree census and  
57 ancillary data, at a multi-hectare scale. Not all data types were collected at all sites, reflecting the practical challenges of field  
58 data collection. We also provide detailed data collection protocols and recommendations for TLS, UAV-LS, ALS and plot  
59 census measurements for each site, along with requirements for ancillary data to enable integration with ALS data (where  
60 possible) and upscaling to EO estimates. We outline the requirements and challenges for field data collection for each data  
61 type and discuss the practical considerations for establishing new FBRMS or upgrading existing sites to FBRMS standard,  
62 including insights into the associated costs and benefits.

63 **1. Introduction**

64 Our capability to estimate forest structure and [AGB](#) has rapidly advanced, leveraging new remote sensing observations from  
65 ground, air, and space. This progress underscores the importance of quantifying and understanding terrestrial carbon sources  
66 and sinks, the response of global forests to climate change, and conservation and restoration efforts at local to global scales.  
67 These new measurements broadly fall into the following categories:  
68

**Deleted:** above-ground biomass (

**Deleted:** )

69 1) [TLS](#) provides highly detailed (centimetre-scale) 3D structural measurements across hectare scales, enabling non-  
70 destructive AGB estimates that are independent of, yet complementary to, empirical allometric model estimates (e.g.  
71 Calders et al., 2022; Demol et al., 2024).

**Deleted:** Terrestrial laser scanning (

**Deleted:** )

82 2) ~~UAV-LS has evolved from highly specialised and expensive surveying platforms to more operational, low-cost~~  
83 systems that offer coverage of several to thousands of hectares, with hundreds to thousands of points per square metre  
84 from above. These data can be used to estimate forest canopy height, basal area, tree crown size and shape, vertical  
85 structure, and AGB via allometric model functions of tree properties, including height, diameter at breast height  
86 (DBH), and crown shape (Brede et al., 2022a; Kellner et al., 2019) However, as UAV-LS systems proliferate, the  
87 need for intercalibration between sensors increases, due to differences in scanner and laser properties such as power,  
88 wavelength, divergence, and scan rate, which result in notable variations in penetration and object detection rates  
89 (Vincent et al., 2023).

90  
91 3) Airborne laser scanning (ALS) has been a well-established tool in forestry and forest ecology since the 1990s. ALS  
92 is routinely used to estimate forest height, structure, and AGB at stand level via empirical models and at regional to  
93 national scales via allometric models (Duncanson et al., 2019; Jucker et al., 2017).

94  
95 4) Spaceborne Light Detection and Ranging ([Spaceborne](#) LiDAR) (e.g. GEDI, ICESat, and ICESat-2) can provide  
96 estimates of forest height in non-continuous footprints of tens to hundreds of metres, underpinning most large-scale  
97 AGB maps, particularly in the lowland tropics (Avitabile et al., 2011; Avitabile et al., 2016; Saatchi et al., 2011).  
98 Various satellite missions have also provided empirical evidence for correlations between the radar signal and AGB  
99 for  $AGB < 250 \text{ Mg ha}^{-1}$  (Askne and Santoro, 2012), but the ESA BIOMASS mission, ~~launched on the 29<sup>th</sup> of April~~  
100 2025, is the only mission specifically targeting higher biomass tropical forests (Quegan et al., 2019; Ramachandran  
101 et al., 2023).

102  
103 The current challenge is to consistently ~~collect~~ and process plot-based measurements in support of EO-derived AGB, combine  
104 them, integrate them with long-term ground-based inventory approaches, and optimally use them with EO data. There is  
105 increasing recognition that the value of large-scale EO approaches to assessing AGB and forest structure largely depends on  
106 robust calibration and validation data (Duncanson et al., 2019; Nature Editorial, 2022; Ochiai et al., 2023). This knowledge  
107 and capability gap have led to calls for concerted international funding and coordination to establish long-term Forest Biomass  
108 Reference Measurement Sites (FBRMS), with a particular focus on tropical forests (Labrière et al., 2023; Schepaschenko et  
109 al., 2019).

110  
111 Here, we present a new dataset from the European Space Agency (ESA) funded ForestScan project, which contributes to this  
112 aim and provides access to data from the first three FBRMS of the GEO-TREES network. The project has collected data,  
113 including TLS, UAV-LS, ALS, and census data, covering three FBRMS across the tropics. We describe these data, related  
114 data collection and processing protocols and tools, and make brief recommendations for future data collection for FBRMS.

**Deleted:** Unpiloted aerial vehicle laser scanning ( )  
**Deleted:**

**Deleted:** scheduled for  
**Deleted:** in  
**Formatted:** Superscript

**Deleted:** make

120 **2. Methodology**

121 **2.1 ForestScan Forest Biomass Reference Measurement Sites (FBRMS)**

122 Three Forest Biomass Research Monitoring Sites (FBRMS) were selected based on various criteria, including the availability  
123 of well-established plots, the representativity of tropical forest types and climates, established collaborations, agreements and  
124 logistical support with in-country partners, and the availability of previously collected data, particularly census data, as well  
125 as ALS and TLS data. The chosen sites were:

- FBRMS-01: Paracou Research Station, French Guiana
- FBRMS-02: Station d'Etudes des Gorilles et Chimpanzés, Lopé National Park, Gabon
- FBRMS-03: Kabili-Sepilok, Malaysian Borneo

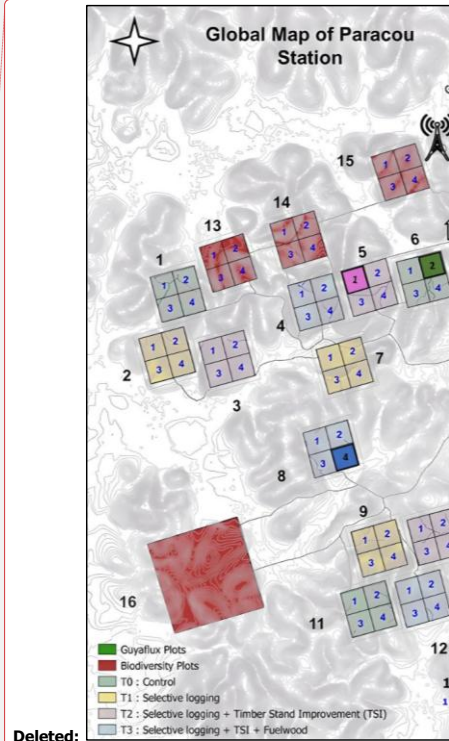
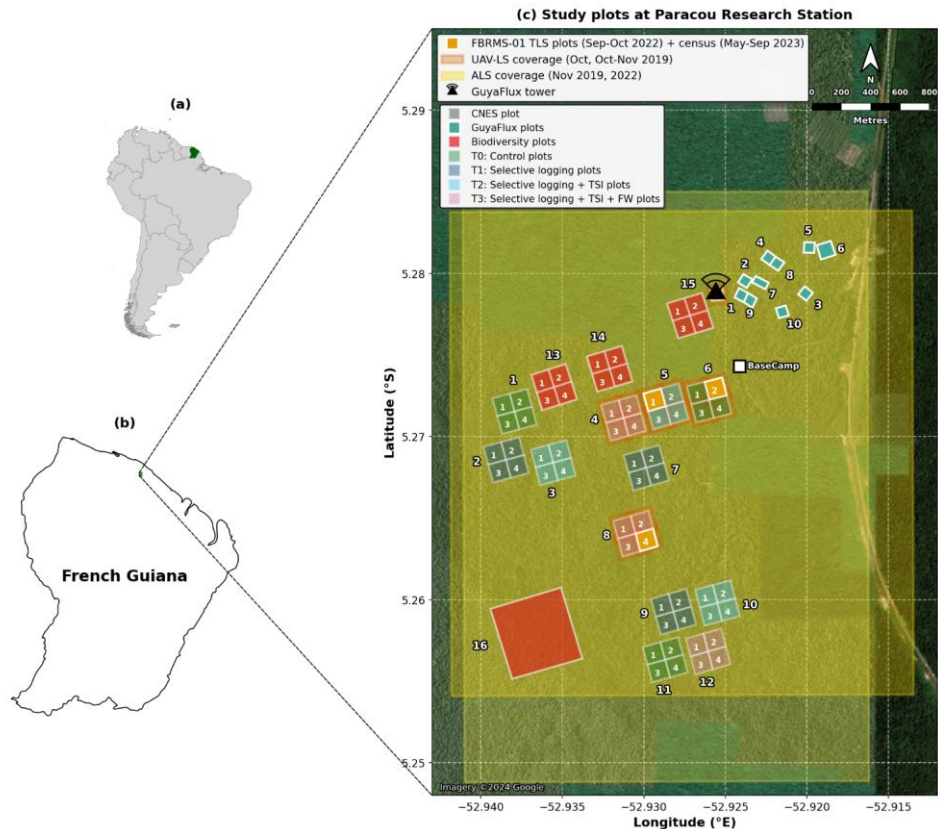
**Deleted:** discussions among the team, the European Space Agency (ESA), external collaborators, and

**Deleted:** Airborne Laser Scanning (

**Deleted:** )

**Deleted:** Terrestrial Laser Scanning (

**Deleted:** )



136  
137 **Figure 1:** Multi-scale map depicting the location and spatial distribution of research plots at Paracou Research Station, French  
138 Guiana. (a) Location of French Guiana (green) within South America. (b) Location of Paracou Research Station (green) within  
139 French Guiana. (c) Detailed site map showing the spatial distribution of research plots with treatment-specific colours, UAV-  
140 LS coverage (orange), and ALS coverage (yellow). The map displays 15 experimental 4 ha plots, each containing four 1 ha  
141 subplots numbered 1 - 4 (60 subplots in total; plots 1 - 12: silvicultural treatments; plots 13 - 15: Biodiversity monitoring), one  
142 large 40 ha Biodiversity plot (plot 16; red), and 10 GuyaFlux plots (solid green). Treatment categories include: Biodiversity  
143 monitoring plots (plots 13, 14, 15, 16; red), T0 Control (plots 1, 6, 11; green), T1 Selective logging (plots 2, 7, 9; dark blue),

Formatted: Font: Not Bold

Formatted: Font: Not Bold

Formatted: Justified

Formatted: Font: Not Bold

145 T2 Selective logging + thinning by timber stand improvement (TSI; plots 3, 5, 10; cyan), and T3 Selective logging + TSI +  
146 fuelwood harvesting/FW (plots 4, 8, 12; pink). The three FBRMS-01 subplots -FG5c1 (subplot 1 of plot 5), FG6c2 (subplot 2  
147 of plot 6), and FG8c4 (subplot 4 of plot 8)- are shown in solid orange and were surveyed using terrestrial laser scanning (TLS)  
148 with corresponding tree census data. The GuyaFlux tower location is indicated by a black triangle with radiating transmission  
149 waves, and the Base Camp location is marked with a white square. Scale bar: 800 m. Map data: Natural Earth 10 m cultural  
150 vectors. Satellite imagery basemap: Imagery ©2024 Google. Map projection: WGS84 (EPSG:4326).

**Formatted:** Font: Not Bold  
**Formatted:** Font: Not Bold

151 ▼  
152  
153 The Paracou research station is located near Sinnamary in the northern part of French Guiana, at a latitude of 5°18'N and a  
154 longitude of 52°53'W. It is established on a long-term concession of the French National Centre for Space Studies (CNES)  
155 and is managed by Centre de Coopération Internationale en Recherche Agronomique pour le Développement-Unité Mixte de  
156 Recherche Écologie des Forêts de Guyane (Cirad-UMR EcoFoG). The station experiences an equatorial climate characterised  
157 by two main climatic periods: a well-marked dry season from mid-August to mid-November and a long rainy season, often  
158 interrupted by a short drier period between March and April. The station receives approximately 3,000 mm of rainfall annually  
159 (mean annual precipitation from 2004 to 2014: 3,102 mm) and has a mean annual temperature of 25.7°C.  
160

161 The core area of the Paracou research station (approximately 500 ha) is predominantly covered by lowland terra firme  
162 rainforest. This old-growth forest has experienced no major human disturbance, although there are signs of pre-Columbian  
163 activities. Species richness is high, with more than 750 woody species recorded, and 150–200 tree species per hectare with  
164 DBH above 10 cm. A few dominant botanical families characterise the vegetation: Fabaceae, Chrysobalanaceae,  
165 Lecythidaceae, Sapotaceae, and Burseraceae. The local heterogeneity of the floristic composition is mainly driven by soil  
166 drainage. AGB, measured on trees with a DBH  $\geq$  10 cm, ranges from 286.10 to 450 Mg/ha.  
167

168 Following an initial inventory in the early 1980s, 12 permanent 6.25 ha plots were established in 1984. Plot corners, perimeters,  
169 and inner trails (defining four subplots) were verified ~10 years later by a professional land surveyor. Nine plots were logged,  
170 and six received additional silvicultural treatments between 1986 and 1988, creating a disturbance gradient with AGB losses  
171 of 18–25% (treatment 1), 40–52% (treatment 2), and 48–58% (treatment 3). In the early 1990s, three more 6.25 ha plots and  
172 one 25 ha plot were added, totalling ~120 ha of forest censused annually (controls), biennially (disturbed plots), or every five  
173 years (25 ha plot). All 6.25 ha plots are subdivided into four subplots (see Fig. 1), with relative tree coordinates recorded. Trees  
174 and palms  $\geq$  10 cm DBH are mapped, identified, tagged, and periodically measured, forming a database of >70,000 trees. Since  
175 2003, a 57 m flux tower has measured greenhouse gas fluxes, and an N, P, NP fertilisation experiment has been ongoing since  
176 2015.

**Deleted:** Map of FBRMS-01: Paracou Research Station, French Guiana (image: Laetitia Proux, UMR EcoFoG). The location of ForestScan plots FG5c1 (pink), FG6c2 (green) and FG8c4 (blue) has been highlighted.

**Formatted:** Font: Not Italic

**Deleted:** a diameter at breast height (

**Deleted:** )

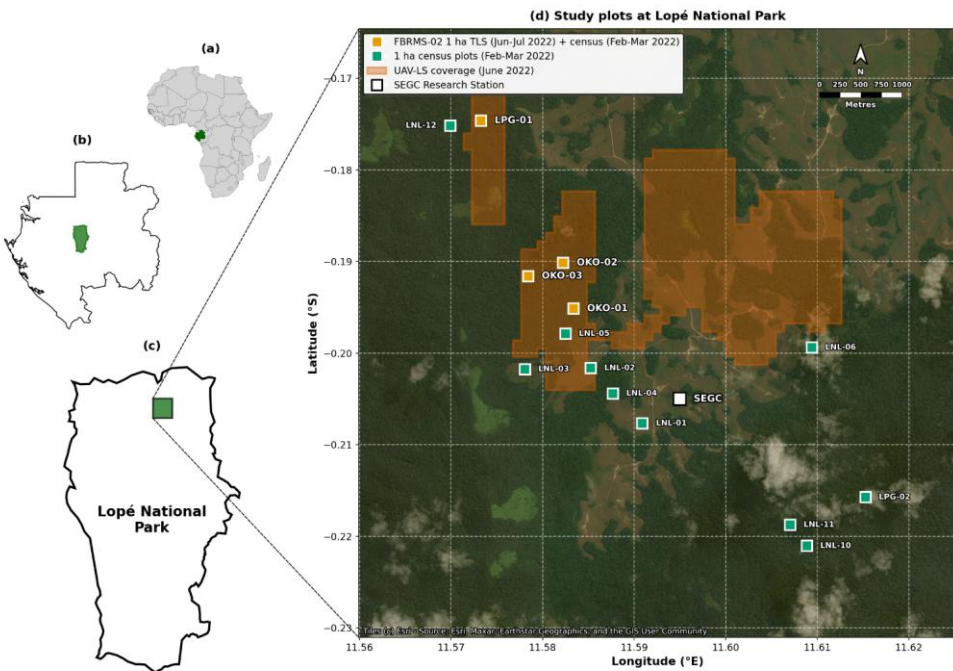
**Deleted:** Aboveground biomass (

**Deleted:** )

**Deleted:** Following an initial large-scale inventory in the early 1980s, 12 permanent plots with an area of 6.25 ha each were established in 1984. The positioning of the plot corners, perimeter, and inner trail (delimiting the four subplots) was verified about 10 years later by a professional land surveyor who confirmed the accuracy of the positioning. Initial tree positioning within plots was done using two tape measures on perpendicular sides of subplots of 12.5 x 12.5 m at the time of plot establishment. Trees recruited after that are positioned relative to the trees present at the time of plot establishment. Nine of the 12 permanent plots were logged, with six receiving additional silvicultural treatment via one of three different treatment modalities between 1986 and 1988. This resulted in a disturbance gradient with a loss of AGB ranging from 18 to 25% for treatment 1, 40 to 52% for treatment 2, and 48 to 58% for treatment 3. In the early 1990s, three new 6.25 ha plots and one 25 ha plot were established, forming a total of about 120 ha of forest censused annually (undisturbed/control plots), every two years (disturbed plots), or every five years (25 ha plot). All 6.25 ha permanent plots are subdivided into four subplots with relative tree coordinates recorded within each subplot (see Fig. 1). Trees and palms with DBH  $\geq$  10 cm are mapped, identified, tagged with a field number unique to their subplot, and periodically measured. This results in a large database covering more than 70,000 trees. Understory woody vegetation (1–10 cm DBH) has been monitored on 64 subplots of 50 m<sup>2</sup> per plot (plots 1–12) since the early 1990s, and a 9 ha permanent plot currently being established in plot 16. Since 2003, the station has had a 57 m flux tower measuring greenhouse gas fluxes. An N, P, NP fertilisation experiment has been ongoing since 2015.

213

## FBRMS-02; Lopé National Park, Gabon

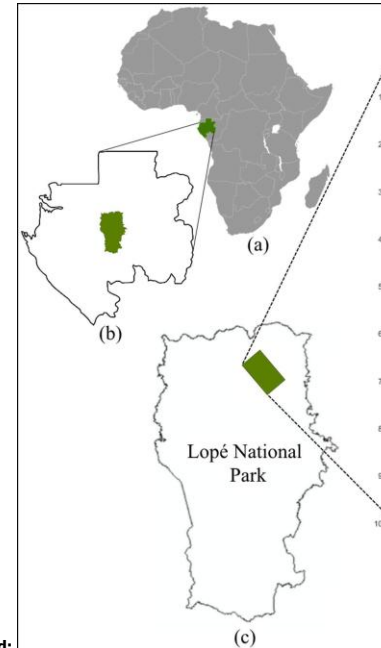


214

215 **Figure 2:** Multi-scale map showing the location and spatial distribution of research plots within Lopé National Park,  
 216 Gabon. (a) Location of Gabon (green) within Africa. (b) Location of Lopé National Park (green) within Gabon. (c) Park  
 217 boundary showing the research site location (green). (d) Detailed site map showing the spatial distribution of 14 one-hectare  
 218 research plots. The four ForestScan FBRMS-02 plots (LPG-01, OKO-01, OKO-02, OKO-03; orange squares) were scanned  
 219 using TLS during Jun-Jul 2022 with tree census data collected during Feb-Mar 2022. Tree census data was also collected for  
 220 another ten plots (green circles) which are not part of the ForestScan project. Orange shaded areas indicate coverage of  
 221 UAV-LS conducted in Jun 2022. The SEGC (Station d'Etudes des Gorilles et Chimpanzés) research station is marked with a  
 222 yellow square. Map data: Natural Earth 10m cultural vectors. Satellite imagery basemap: Esri World Imagery (Esri, Maxar,  
 223 Earthstar Geographics, and the GIS User Community). Map projection: WGS84 (EPSG:4326).

224  
 225 Lopé National Park is a 5000 km<sup>2</sup> protected area in central Gabon (Latitude 0°30'S  
 226 and Longitude 11°30'E), comprising predominantly intact old-growth moist tropical forest. The northern part of the park  
 227 features a savanna-forest mosaic, an anthropogenically maintained remnant of the landscape from the Last Glacial Maximum.  
 228 The broader landscape is designated as a UNESCO World Heritage Site.

**Deleted:** Station d'Etudes des Gorilles et Chimpanzés,



**Deleted:**

**Deleted:** coordinates: -0.5° latitude, 11.5° longitude; see Fig. 2

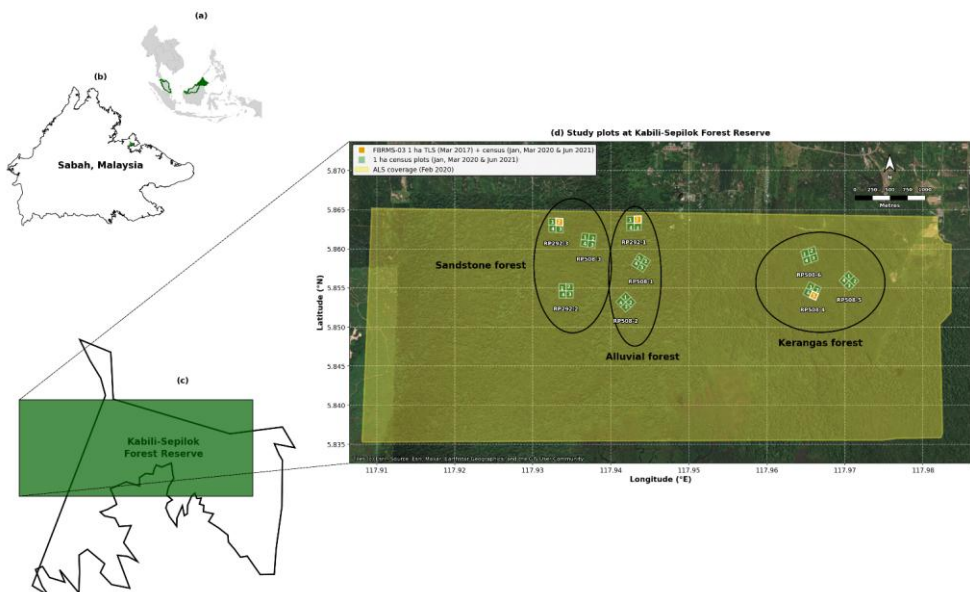
237

238 The transition from savanna to old-growth forest in the northern part of the park is characterised by six distinct forest types  
 239 (Cuni-Sanchez et al., 2016; White et al., 1995): (i) savanna, (ii) colonising forest, (iii) monodominant Okoume forest, (iv)  
 240 young Marantaceae forest, (v) mixed Marantaceae forest, and (vi) old-growth forest.

241

242 A substantial and varied body of literature has emerged from research conducted in Lopé National Park (Agence Nationale  
 243 Des Parcs Nationaux, 2025). More than 100 long-term censused forest plots have been established within the park, contributing  
 244 significant ground data for the calibration and validation of EO instruments (i.e. Duncanson et al., 2022; Saatchi et al., 2019).  
 245 These plots also support various other research activities, such as the Global Ecosystem Monitoring (GEM) Network, an  
 246 initiative aimed at understanding forest ecosystem functions and traits (Malhi et al., 2021).

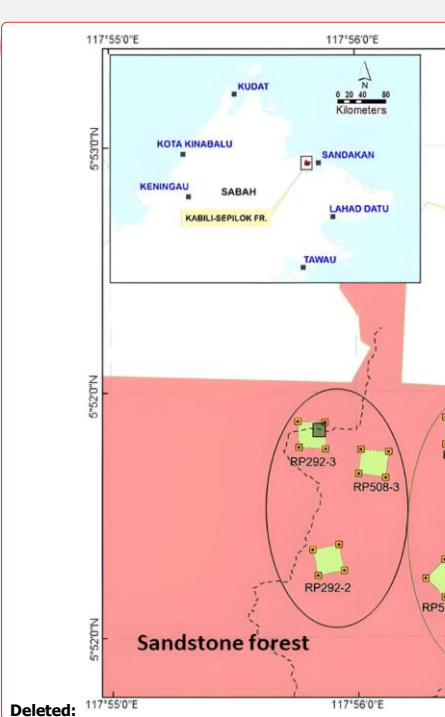
247 **FBRMS-03: Kabil-Sepilok, Malaysian Borneo**



248  
 249 **Figure 3:** Multi-scale map showing the location and spatial distribution of research plots at Kabil-Sepilok Forest Reserve,  
 250 [Sabah, Malaysian Borneo](#). (a) Location of Sabah (green) within Malaysia (green boundary) in Southeast Asia. (b) Location  
 251 [of the Kabil-Sepilok Forest Reserve](#) (green) within Sabah. (c) Kabil-Sepilok Forest Reserve area and site map area of panel

**Deleted:** Earth Observation (

**Deleted:** )



**Deleted:**

255 d (green rectangle). (d) Detailed site map showing the spatial distribution of 9 x 4 ha plots (labelled RP291-1, RP292-3, etc.)  
256 each containing four 1 ha subplots numbered 1 - 4 (36 subplots in total; green polygons with white subplot numbers) across  
257 three soil types: Alluvial forest, Sandstone forest, and Kerangas forest (delineated by black ellipses). The three FBRMS  
258 subplots are SEP-11 (subplot 2 of plot RP292-3, sandstone soil), SEP-12 (subplot 2 of plot RP292-1, alluvial soil) and SEP-  
259 30 (subplot 3 of plot RP508-4, kerangas soil). Three ForestScan FBRMS-03 1 ha subplots (orange polygons) were scanned  
260 using TLS during March 2017 and tree census for all subplots was collected in Jan, Mar of 2020 and Jun 2021. Yellow  
261 shading indicates ALS coverage acquired in February 2020. Scale bar: 1000 m. Map data: Natural Earth 10m cultural  
262 vectors. Satellite imagery basemap: Tiles ©Esri - Source: Esri, Maxar, Earthstar Geographics, and the GIS User Community.  
263 Map projection: WGS84 (EPSG:4326).

264 The Kabili-Sepilok Forest Reserve is located on the Sandakan Peninsula in North-East Sabah, Malaysia, and encompasses  
265 approximately 4,300 hectares of intact old-growth tropical forest. Sepilok has been protected since its establishment by the  
266 Sabah Forest Department in 1931. The elevation ranges from 50 to 250 metres above sea level. This topographic variation,  
267 combined with edaphic differences, results in three distinct forest types: (i) lowland mixed dipterocarp forest overlaying  
268 alluvial soil in the valleys, (ii) sandstone hill forest on hillsides and crests, and (iii) lowland mixed dipterocarp and kerangas  
269 forest at higher elevations (Sabah Forestry Department, n.d.).

270  
271 Between 1995 and 2000, the Ecology Section of the Sabah Forestry Department established 36 one-hectare censused forest  
272 stands across these forest types, as illustrated in Fig. 3.

## 273 2.2 Data

### 274 2.2.1 Tree census

275 Quality-controlled, tree-by-tree data on identity (tag number and species) and diameter size for all sampled plots in each of the  
276 three FBRMS were collected using global standard tropical forest plot inventory protocols (Forestplots.Net et al., 2021). This  
277 ensured a consistent, full species-level census for all plot trees with a diameter equal to or greater than 10 cm at each FBRMS.  
278 Censuses provide tree-by-tree records that can potentially be linked to laser-scanning approaches. Species identity plays a key  
279 role in determining tree biomass through its strong influence on wood density. While laser-scanning techniques provide  
280 excellent measurements of tree dimensions (such as height and volume), they still require wood density estimates to convert  
281 these volumes into accurate biomass values (see Goodman et al., 2014). Census data also provide tree-by-tree measurements  
282 of tree diameter and whole forest basal area. Finally, because they are independent of constantly changing sensor technologies,  
283 when sustained over time, the core measurement protocols in forest plots deliver long-term consistency for tracking forest  
284 biomass change, growth, mortality, demography, and their trends over decades.

285  
286 Census data for FBRMS plots in Gabon and Malaysia are available via ForestPlots.net (<https://forestplots.net/>, Forestplots.Net  
287 et al., 2021; Lopez-Gonzalez et al., 2011). ForestPlots.net is an internet-based facility with functionality to support all aspects  
288 of forest plot data management, including archiving, quality control, sharing, analysis, and data publishing via stable URLs

**Deleted:** Map and location of the 36 x 1 ha forest plots established across the three distinct forest types found in FBRMS-03: Kabili-Sepilok, Malaysian Borneo. Map adapted with permission from Sabah Forestry Department (Sabah Forestry Department, n.d.) to show the location of ForestScan plots SEP-11 (Sandstone forest), SEP-12 (Alluvial forest) and SEP-30 (Kerangas forest).

**Deleted:** Goodman et al.

**Deleted:** Species identity exerts critical control on tree biomass via its strong influence on wood density. Laser-scanning techniques can provide excellent measures of dimensions (e.g., height, volume) but require wood density estimates to convert tree volume into tree biomass (see Fig. 4)

301 (DOIs). ForestPlots.net currently supports the data management needs of more than 2,000 contributors working with 7,000  
302 plots across 23 participating tropical networks. Data access requires potential users to provide details of their planned use and  
303 agreement to abide by requirements for the inclusion of all contributing researchers. This encourages maximum inclusivity of  
304 data originators and is recognised as a key part of what is required to maintain long-term investment in people and infrastructure  
305 that enables continued measurements in these areas (De Lima et al., 2022).

306 **Tree census: FBRMS-01: Paracou, French Guiana**

**Deleted:** 1

307 In the Paracou FBRMS, tree censuses are conducted by two teams of three to five permanent field staff using Qfield on field  
308 tablets (since 2020, field computers were used prior to this). Tree girth is measured with a measuring tape at 1.3 m, except  
309 when buttresses necessitate a higher measurement point. The point of measurement (POM) is marked with paint to ensure the  
310 exact same point of measurement between censuses. POM and its potential changes are recorded. New recruits -trees that have  
311 grown beyond 10 cm DBH since the previous survey- are recorded by the field team using vernacular names, and their positions  
312 are measured relative to the original trees. To ensure accurate identification, periodic botanical campaigns are conducted by  
313 one or two experienced botanists, who also correct any misidentifications. When species cannot be identified in the field,  
314 samples are collected and examined at the EcoFoG herbarium in Kourou or the IRD herbarium in Cayenne. All identifications  
315 follow the Angiosperm Phylogeny Group (APG) IV plant classification system. Dead trees and the cause of their death are  
316 recorded. Data are checked for errors after field census using an R script. Any abnormal measurement (e.g., girth showing  
317 abnormal increase/decrease, missing value) is then rechecked in the field in the weeks following the initial census.

**Deleted:** New recruits (i.e., trees that have exceeded 10 cm DBH since the previous survey) are recorded and identified by vernacular names by the field team. Their position is measured relative to initial trees....

318  
319 Plot descriptions for the Paracou FBRMS plots FG5c1, FG6c2 and FG8c4, are accessible via the Guyafor DataVerse  
320 (<https://dataVERSE.cirad.fr>). This internet-based data repository provides plot descriptions and datasets downloadable as CSV  
321 files, together with the corresponding metadata. (Derroire et al., 2023). The ForestScan Project data package, including the  
322 latest tree census data used in our analysis and collected in August 2023 for FBRMS plot FG5c1, in June 2023 for plot FG6c2,  
323 and in September 2023 for plot FG8c4, is accessible via  
324 <https://dataVERSE.cirad.fr/dataset.xhtml?persistentId=doi:10.18167/DVN1/94XHID> (Derroire et al., 2025).

**Deleted:** 1

**Deleted:**

**Deleted:** [dataset.xhtml?persistentId=doi:10.18167/DVN1/94XHID](https://dataset.xhtml?persistentId=doi:10.18167/DVN1/94XHID)

**Deleted:** 1

...

**Field Code Changed**

**Deleted:** , referenced by a DOI

325 **Tree census: FBRMS-02: Lopé, Gabon**

326 In the Lopé FBRMS, tree census data was collected at 12 plots in 2017 for the ESA AfriSAR campaign. During June - July  
327 2022, these 12 plots plus one additional 1 ha plot (LPG-02) were re-censused, making a total of 13 x 1 ha forest plots, plus 3  
328 x 1 ha plots in savanna (see Fig. 2). The 10 ha plots included LPG-01, OKO-01, OKO-02 and OKO-03, the 4 x 1 ha FBRMS  
329 plots where TLS was conducted in 2017 and 2022.

**Deleted:** 2

**Deleted:** 0

**Deleted:** llect

351 **Tree census: FBRMS-03: Kabili-Sepilok, Malaysian Borneo**

352 In the Kabili-Sepilok FBRMS, tree census data was collected during 2020 - 2022 for a total of ~~9 x 4 ha plots (IDs RP291-1,~~  
353 ~~RP292-3, etc. see Fig. 3)~~ each containing four 1 ha subplots numbered 1 - 4 and covering most of the long-term plots at this  
354 site. ~~The three FBRMS subplots SEP-11 (subplot 2 of plot RP292-3, sandstone soil), SEP-12 (subplot 2 of plot RP292-1,~~  
355 ~~alluvial soil) and SEP-30 (subplot 3 of plot RP508-4, kerangas soil) were scanned using TLS during March 2017 and tree~~  
356 ~~census for all subplots was collected in Jan, Mar of 2020 and Jun 2021. The 2020-2022 census was overdue as these plots had~~  
357 not been censused since 2013.

**Deleted:** 9 x 4 ha plots

358 Plot meta-data, including geography, institution, personnel and historical context, as well as tree-level census attributes (tag,  
359 identity, diameter, point of measurement, stem condition, height, sub-plot, and, where measured x, y coordinates of 5 x 5 m  
360 subplots) and multi-census attributes (tree demography and measurement trajectory and protocols, including growth, point of  
361 measurement changes, recruitment, mortality, and mortality mode) were recorded for all Gabon~~ese~~ and Malaysian~~n~~ FBRMS  
362 plots.

**Deleted:** These 4 ha plots included SEP-11, SEP-12, and SEP-30, the 3 x 1 ha FBRMS plots where TLS was collected in 2017.

**Deleted:** A 2 ha plot, one of the oldest in the global tropics, dating back to 1958 (RP-17 = SEP-06, sandstone forest) was also censused.

364  
365 The ForestScan Project data package, includes data from the 2022 tree census collected during February and March for the  
366 Gabon FBRMS plots and the Malaysian FBRMS plots census data collected in October 2020 for FBRMS plot SEP-11, in  
367 March 2020 for plot SEP-12, and in June 2021 for plot SEP-30. This data package can be accessed via  
368 [https://doi.org/10.5521/forestplots.net/2025\\_2](https://doi.org/10.5521/forestplots.net/2025_2) (Chavana-Bryant et al., 2025).

369 **2.2.2 Terrestrial Laser Scanning (TLS)**

370 ~~TLS~~ data was collected to provide state-of-the-art estimates of tree- and stand-scale AGB for each FBRMS. These LiDAR  
371 measurements, collected using the protocol described in the following sections, produce 3D point clouds ~~with millimetre-level~~  
372 ~~accuracy~~, representing the forest at each FBRMS. ~~TLS~~ chain sampling ~~protocols~~ (Wilkes et al., 2017), as illustrated and  
373 described in Fig. 4, ~~were~~ employed at all three FBRMS. This data was processed to construct explicit Quantitative Structural  
374 Models (QSMs) describing individual trees within each FBRMS with a ~~DBH~~  $\geq 10$  cm. Tree- and stand-scale AGB estimates  
375 were then calculated from the volumes of these models, using wood density values derived from published sources based on  
376 species identification from botanical surveys.

**Deleted:** iDAR

**Deleted:** terrestrial LiDAR

**Deleted:** above-ground biomass (

**Deleted:** )

**Deleted:** Forest Biomass Research Monitoring Site (

**Deleted:** )

**Deleted:** millimetre-accurate

**Deleted:** /digital twins

**Deleted:** Terrestrial Laser Scanning (

**Deleted:** )

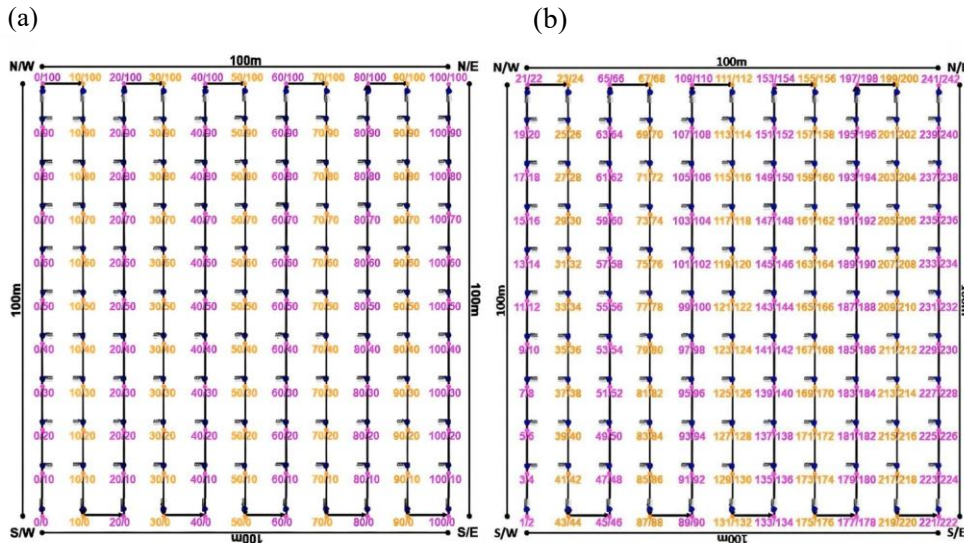
**Deleted:** 5

**Deleted:** as

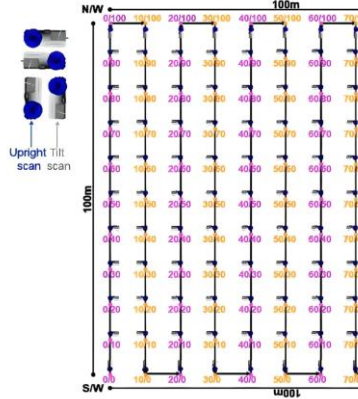
**Deleted:** stem diameter

**Deleted:**

402  
403  
404  
405  
406  
407



408  
409 **Figure 4.** TLS chain sampling was employed to capture high-quality LiDAR data suitable for accurate tree- and stand-scale  
410 AGB estimation. Chain sampling was deployed over a 10 m Cartesian grid, resulting in 11 sampling lines with 11 scan  
411 positions along each line (i.e., 0 – 10) within 1 ha forest plots. Sampling lines were established in a south-to-north direction  
412 (standard practice) and colour-coded using flagging tape, with the ID of each scan position written in permanent marker. Scan  
413 positions were identified by their line number and grid position, as shown in panel b (left). Due to the scanner's 100° field of  
414 view, capturing a complete scene at each scan position required two scans—upright and tilted. Consequently, 242 scans were  
415 collected from 121 positions at each 1 ha forest plot. The order in which the 242 individual scans were collected at each plot  
416 is depicted in panel b (right). The first scan at each plot was collected at the southwest corner, i.e., scan position 0,0 (unless  
417 impeded by obstacles such as streams, large tree falls, etc., or if the plot was oriented differently). To facilitate scan registration,  
418 all tilt scans along the first sampling line were oriented towards the same sampling position along the next sampling line, and  
419 all other tilt scans along plot edges were oriented towards the inside of the plot so that the previous scan location was within



**Deleted:**  
**Deleted:** 5a & b  
**Deleted:** Terrestrial LiDAR Scanning (   
**Deleted:** )  
**Deleted:** above-ground biomass (   
**Deleted:** )  
**Deleted:** 5  
**Deleted:** 5  
**Deleted:** c

429 the tilt-scan field of view. Depending on the density of the canopy understorey, terrain, and wind conditions (ideally, low to  
430 zero wind and no rain or mist/fog), a team of three experienced TLS operators required 1–2 full working days (8 hrs per day)  
431 to set up the chain sampling grid and 3–5 full days to complete the scanning of a 1 ha plot.

432

433 TLS data for all three FBRMS were collected using a RIEGL VZ-400 laser scanner or its newer model, the VZ-400i, which  
434 has very similar technical specifications (see Table 1) and includes Global Navigation Satellite System (GNSS) Real-Time  
435 Kinematic (RTK) positioning (RIEGL Laser Measurement Systems GmbH, 2025). RTK GNSS facilitates TLS data acquisition  
436 by replacing the labour-intensive and time-consuming task of placing and continuously relocating retro-reflective targets  
437 between scan positions as required by the RIEGL VZ-400 scanner. Common targets between adjacent scan locations were  
438 later identified and used to create a registration chain that integrates the 3D point cloud of a scanned plot. GNSS RTK has  
439 replaced the use of common targets, enabling the absolute (latitude, longitude, and altitude) and relative (between base and  
440 rover GNSS) positioning of individual scans with centimetre precision, which makes the auto-registration of scans in real-time  
441 possible. This GNSS-enabled auto-registration significantly reduces the time and effort required to both collect and register  
442 TLS data. Furthermore, data collected with the VZ-400i are backwards compatible with data from the older VZ-400 scanner,  
443 allowing for consistent processing and comparison over time.

444

445 **Table 1:** Characteristics of RIEGL laser scanners (RIEGL Laser Measurement Systems GmbH, 2025) used for TLS data  
446 acquisition at ForestScan FBRMS.

Characteristic	RIEGL VZ-400	RIEGL VZ-400i
Max Pulse Repetition Rate [kHz]	300 – 1200 (300 used)	300 – 1200 (300 used)
Angular resolution	0.04° (22.4 million emitted pulses per scan, i.e. 5.42 billion per hectare)	0.04° with 22.4 million emitted pulses per scan (5.42 billion per hectare)
Wavelength [nm]	~1550 (near-infrared)	~1550 (near-infrared)
FOV [°]	360 (horizontal)	360 (horizontal)
Ranging accuracy / precision [mm]	5 / 3	5 / 3
Max range [m]	~800 @ 80% reflectivity	~800 @ 80% reflectivity
Beam divergence [mrad]	0.35	0.35
Beam diameter at emission [mm]	7	7
Returns per pulse	Up to 7	Unlimited (waveform)
Scan time per scan	3 minutes	3 minutes

Moved (insertion) [1]

Deleted: Forest Biomass Research Monitoring Sites (

Deleted: )

<u>GNSS RTK positioning</u>	<u>No</u>	<u>Yes (integrated)</u>
<u>Weight [kg]</u>	<u>~13</u>	<u>~13</u>
<u>Operated by</u>	<u>UCL</u>	<u>UCL</u>
<u>Scan site (s)</u>	<u>FBRMS-03: Malaysia</u>	<u>FBRMS-01: French Guiana</u> <u>FBRMS-01: Gabon</u>

449

450 **TLS: FBRMS-01: Paracou, French Guiana**

451 ~~TLS~~ data was collected in Paracou over two separate periods due to interruptions caused by the COVID-19 pandemic. The  
 452 ~~first campaign took place in 2019, censused plot FG6c2 was scanned with a RIEGL VZ-400 scanner during October and~~  
 453 ~~November~~ (Brede et al., 2022a). The scanning was conducted over a 200 x 200 m<sup>2</sup> area (i.e. two 1 ha plots) covering two of  
 454 ~~plot 6 subplots -2 and -4- (see Panel c in Fig. 1)~~, resulting in 21 x 21 scan lines with 10 m grid spacing. Retro-reflective targets  
 455 ~~were placed between scan positions to facilitate coarse registration (Wilkes et al., 2017).~~

456

457 ~~The second TLS campaign took place in 2022, three 1 ha censused plots (see Fig. 1) were scanned during September and~~  
 458 ~~October using a RIEGL VZ-400i scanner with GNSS RTK-enabled auto-registration. These plots were selected to represent~~  
 459 ~~the disturbance gradient found at this site, as shown in Table 2. All three plots were also scanned with ALS and plot FG6c2~~  
 460 ~~additionally scanned with UAV-LS.~~

461

462 **Table 2:** Overview of plots scanned in 2022 with TLS in Paracou, French Guiana.

Plot ID	Subplot	Logging treatment	Description	AGB	Lat	Long
FG6c2	2	Control	Old-growth, lowland, Terra firme rainforest	High	5.27	-52.92
FG5c1	1	T2	Old-growth, lowland, Terra firme rainforest with mid-level logging disturbance	Mid	5.27	-52.92
FG8c4	4	T3	Old-growth, lowland, Terra firme rainforest with high-level of logging disturbance	Low	5.26	-52.93

463

**Deleted:** Terrestrial LiDAR Scanning (

**Deleted:** )

**Deleted:** In 2019, censused plot FG6c2 was scanned during October and November

**Deleted:** equivalent to 16 quarter

**Deleted:** -hectare

**Deleted:** FG6 subplots

**Deleted:** A

**Deleted:** IEGL VZ-400 scanner (RIEGL Laser Measurement Systems GmbH, 2025) was used, with r

**Deleted:** 1

**Deleted:** in Paracou

**Deleted:** (RIEGL Laser Measurement Systems GmbH, 2025)

**Deleted:** 1

**Deleted:** below

**Deleted:** also

**Deleted:** 1

**Moved up [1]:** TLS data for all three Forest Biomass Research Monitoring Sites (FBRMS) were collected using a RIEGL VZ-400 laser scanner or its newer model, the VZ-400i, which has very similar technical specifications and includes Global Navigation Satellite System (GNSS) Real-Time Kinematic (RTK) positioning (RIEGL Laser Measurement Systems GmbH, 2025). RTK GNSS facilitates TLS data acquisition by replacing the labour-intensive and time-consuming task of placing and continuously relocating retro-reflective targets between scan positions as required by the RIEGL VZ-400 scanner. Common targets between adjacent scan locations were later identified and used to create a registration chain that integrates the 3D point cloud of a scanned plot. GNSS RTK has replaced the use of common targets, enabling the absolute (latitude, longitude, and altitude) and relative (between base and rover GNSS) positioning of individual scans with centimetre precision, which makes the auto-registration of scans in real-time possible. This GNSS-enabled auto-registration significantly reduces the time and effort required to both collect and register TLS data. Furthermore, data collected with the VZ-400i are backwards compatible with data from the older VZ-400 scanner, allowing for consistent processing and comparison over time.¶

502 **TLS: FBRMS-02: Lopé, Gabon**

503 TLS data was collected in 2022, four 1 ha plots were scanned using a RIEGL VZ-400i with GNSS RTK-enabled auto-  
 504 registration, eliminating the need for retro-reflective targets between scan positions. The four sampled plots, shown in Table  
 505 3, were selected to represent the diversity of forest types found within this site.

507 **Table 3:** Overview of plots scanned with TLS in Lopé National Park, Gabon.

Plot ID	Description (local plot name / forest type)	Lat	Long
LNL-07	OKO-01 / Maturing secondary Okoumé forest	-0.19	11.58
LNL-08	OKO-02 / Maturing secondary Okoumé-Sacoglottis forest	-0.19	11.58
LNL-09	OKO-03 / Maturing secondary Okoumé forest	-0.19	11.57
LPG-01	Angak / Old-growth forest	-0.17	11.57

509 **TLS: FBRMS-03: Kabili-Sepilok, Malaysian Borneo**

510 TLS data was collected for three 1 ha forest plots at this FBRMS during March 2017. The three sampled plots, shown in Table  
 511 4, were selected to represent the three distinct forest types found within this site. A RIEGL VZ-400 scanner was used, with  
 512 retro-reflective targets positioned between scan locations to facilitate coarse registration (Wilkes et al., 2017).

514 **Table 4:** Overview of plots scanned with TLS in Kabili-Sepilok Forest Reserve, Malaysia. Note: subplot 2 was

Plot ID	Subplot	Description (local plot name / forest type)	Lat	Long
SEP-11	2	292/3 / Sandstone forest	5.86	117.94
SEP-12	2	292/1 / Alluvial forest	5.86	117.93
SEP-30	3	508/4 / Kerangas forest	5.86	117.97

516 **TLS data processing**

517 TLS data was collected and processed to provide state-of-the-art estimates of tree- and plot-scale structural attributes and AGB  
 518 for each ForestScan FBRMS. Five main processing steps are required to retrieve structural attributes from the acquired TLS  
 519 data are described below. These processing steps demand significant computational resources - a full 1 ha plot can take 3.4 to

**Deleted:** Both the RIEGL VZ-400 and VZ-400i scanners are time-of-flight, multiple-return, waveform instruments operating in the near-infrared. These instruments have generally been used with an angular resolution of 0.04° in dense forests, resulting in approximately 22.4 million emitted pulses per scan (i.e., 5.42 billion per hectare). While angular resolution can be increased, scanning time also increases linearly, this choice is therefore a compromise. Up to seven returns can be resolved per pulse, with a nominal ranging accuracy of 5 mm. The laser itself is characterised by a beam divergence of 0.35 mrad, and the diameter of the beam at emission is 7 mm (e.g., the diameter of the beam at a range of 50 m would be 21 mm). The pulse repetition rate can be set between 300 and 1200 kHz, but higher scan rates use lower power returns. In this study, a rate of 300 kHz was used, with each scan taking approximately 3 minutes to complete at this rate.¶

**Moved down [2]:** The four sampled plots, shown in Table 2, were selected to represent the diversity of forest types found within this site. A RIEGL VZ-400 scanner

**Deleted:** Lopé over two separate periods due to interruptions caused by the COVID-19 pandemic. In 2016, four 1 ha censused plots were scanned during July and August. The four sampled plots, shown in Table 2, were selected to represent the diversity of forest types found within this site. A RIEGL VZ-400 scanner (RIEGL Laser Measurement Systems GmbH, 2025) was used, with retro-reflective targets positioned between scan locations to facilitate coarse registration (Wilkes et al., 2017). In

**Deleted:** the same

**Deleted:** re

**Moved (insertion) [2]**

**Deleted:** 2

**Deleted:** 2

**Deleted:** 3

**Deleted:** TLS data was collected Subplot 2 was scanned with TLS for plots SEP-11 and SEP-12 and subplot 3 in SEP-30.¶

**Deleted:** (RIEGL Laser Measurement Systems GmbH, 2025)

**Deleted:** 3

**Deleted:** terrestrial LiDAR

**Deleted:** above-ground biomass (

**Deleted:** )

560 4 days to process from start to finish on a high performance computing (HPC) cluster, running on multiple central processing  
561 units (CPUs; general-purpose processors optimised for sequential tasks and complex logic) and graphics processing units  
562 (GPUs; highly parallel processors ideal for deep learning, point cloud processing and simulations tasks that can be broken into  
563 thousands of simultaneous operations).

### 565 1. Individual scan registration into plot-level point cloud

566 This process was carried out using retro-reflective targets positioned between scan locations to facilitate coarse registration for  
567 data collected with the RIEGL VZ-400 or in a near-automated manner using the RIEGL VZ-400i's GNSS RTK positioning  
568 capabilities in conjunction with the enhanced RIEGL RiSCAN Pro software (versions 2.14–2.17). The integrated Auto  
569 Registration 2 (AR2) function employs GNSS RTK data to update the scanner's position and orientation, including in tilt  
570 mode, thereby enabling real-time automated coarse registration during scanning. Major registration errors are easily detected,  
571 typically occurring during pre-processing in RiSCAN Pro when individual scans fail to register (i.e., no coherent solution is  
572 found) or are incorrectly positioned, which is visually apparent. In cases where coarse registration/auto-registration fails,  
573 unregistered scans can be identified, adjusted, and refined using Multi Station Adjustment 2 (MSA2). Following this workflow,  
574 the co-registration of all TLS point clouds achieves sub-centimetre accuracy, as confirmed through post-registration inspection.  
575 Wind and occlusion are key sources of uncertainty for the scan registration process, highlighting the necessity of scanning  
576 under low or zero wind conditions and capturing both tilt and upright scans at each location.

577 The use of GNSS significantly enhances the utility and accessibility of TLS by drastically reducing both data acquisition and  
578 processing time. This is achieved by (1) as previously mentioned, replacing the previous labour-intensive and time-consuming  
579 practice of using common retro-reflective targets to link adjacent scan positions into a registration chain (Wilkes et al., 2017),  
580 and (2) reducing the manual processing registration time by an experienced user to 1 - 2 days per hectare, which is less than  
581 half the time required when using retro-reflective targets.

583 Registration results in a plot-level point cloud, comprising 242 individual scan-level point clouds, potentially containing more  
584 than 5.42 billion points. ▾

586 The subsequent four processing steps were performed in a semi-automated manner using the *rxp-pipeline* (Wilkes and Yang,  
587 2025a) and *TLS2trees* processing pipelines (Wilkes et al., 2023) and *TreeOSM* version 2.3 (Raumonen et al., 2013), as  
588 described below.

**Moved down [6]:** designed to automate tree extraction from TLS point clouds, utilising high-performance computing (HPC) facilities, particularly GPUs (Wilkes et al., 2023). By automating the

**Deleted:** (Wilkes and Yang, 2025)(PDAL Contributors, 2020)TLS data was processed using the *TLS2trees* processing pipeline (Wilkes et al., 2023; Wilkes et al., 2024). *TLS2trees* is a set of free and open...

**Deleted:** The five main processing steps required to retrieve structural attributes from the acquired TLS data are described below. These processing steps demand significant computational resources...

**Deleted:** This process was conducted in a near-automated manner using the RIEGL VZ-400i's new GNSS RTK positioning capabilities and the enhanced RIEGL RiSCAN software (versions 2.14 - 2.17)...

**Deleted:** Following

**Deleted:** r

**Deleted:** ,

**Deleted:** was generated for each of the scanned FBRMS plots

**Deleted:** A small section of the plot-level point cloud collected from a forest stand in Paracou, French Guiana, is shown in Fig. 6.



**Deleted:**

**Deleted:** Figure 6: A section of plot-level point cloud coloured by height (0 - 45m) from plot FG6c2 in FBRMS-01: Paracou.¶

**Deleted:** the

**Formatted:** Font: Italic

**Formatted:** Font: Italic

655 2. Pre-processing of plot-level point clouds

656 Pre-processing is carried out in three steps using the open-source tool *rxp-pipeline* (Wilkes and Yang, 2025a), which operates  
657 directly on the raw RIEGL scan data. First, the co-registered RIEGL point clouds are filtered to remove points with a deviation  
658 greater than 15 and reflectance outside the range [-20, 5]. The data are then clipped to the plot extent, with an additional 10 m  
659 around the plot, segmented into 10 m x 10 m tiles, and converted from the RIEGL proprietary .rxp to .ply format to enable  
660 further processing. Second, to reduce computing load, the tiled point clouds are downsampled using a voxelisation approach  
661 with a voxel size of 0.02 m, implemented via *PDAL.VoxelCenterNearestNeighbor* filter (PDAL Contributors, 2025). Finally,  
662 a tile index mapping the spatial location of each tile is generated. In a HPC system, preprocessing of a 1 ha plot can take 1.58  
663 to 4.17 hours to complete.

664 3. Semantic segmentation: wood-leaf separation

665 *TLS2trees* is an open-source Python command-line pipeline (Wilkes et al., 2025), designed to automate tree extraction from  
666 TLS point clouds by utilising GPUs for parallel computation, making it fully scalable on HPC systems (Wilkes et al., 2023).  
667 The first of the two-step *TLS2trees* workflow employs a deep-learning based approach, implementing a modified version of  
668 the Forest Structural Complexity Tool (FSCT) semantic segmentation method by Krisanski et al. (2021) to classify points  
669 within tiled point clouds into homogeneous classes representing distinct biophysical components: leaf, wood, coarse woody  
670 debris, or ground. An example of the wood and leaf classes extracted from tree-level point clouds is illustrated in Fig. 5. In a  
671 HPC system, semantic segmentation of a 1 ha plot can take 4 to 12 hours to complete.



673  
674 Figure 5: Tree-level point cloud of the largest *Baillonella toxisperma* (Maobi) tree (~40 m tall with an almost circular  
675 canopy ~50 m wide) in plot LPG-01, FBRMS-02: Lopé, Gabon. Points are classified and displayed by category only: wood  
676 points in brown and leaf points in green.

<b>Moved (insertion) [5]</b>
<b>Deleted:</b> accomplished through a three-step procedure
<b>Deleted:</b> .
<b>Formatted</b>
<b>Moved up [5]:</b> Pre-processing is accomplished through a three-
<b>Deleted:</b> Initially, the point clouds are clipped to the plot extent
<b>Moved (insertion) [6]</b>
<b>Formatted</b>
<b>Deleted:</b> .
<b>Deleted:</b> high-performance computing (
<b>Deleted:</b> )
<b>Deleted:</b> facilitie
<b>Deleted:</b> , particularly GPUs
<b>Field Code Changed</b>
<b>Deleted:</b> By automating the previously time-consuming process
<b>Deleted:</b> <i>TLS2trees</i>
<b>Deleted:</b> s
<b>Formatted</b>
<b>Deleted:</b> groups or
<b>Deleted:</b> of different
<b>Deleted:</b> 7 below
<b>Deleted:</b> 7
<b>Deleted:</b> Wood (brown) and leaf (green) points in tree-level poi

710 4. Instance segmentation: individual tree separation

711 The second step in the [TLS2trees](#) workflow, identifies and segments individual trees via a 2-step process. The Dijkstra's shortest  
712 path method first groups all points identified as wood into a set of individual woody stems to which points identified as leaf  
713 are then assigned. A small group of trees automatically segmented from a plot in Gabon are shown in Fig. 6. In a HPC system,  
714 instance segmentation of a 1 ha plot can take 15-20 hours to complete.  
715



716 **Figure 6:** Individual tree-level point clouds acquired from plot LPG-01 in FBRMS-02: Lopé, Gabon.

717 5. TreeQSM: quantitative structural models and results

718 Quantitative structural models (QSMs) were constructed in a near-automated manner from each [individually segmented](#) tree  
719 [point cloud \(woody components only\)](#) with a DBH  $\geq 10$  cm within each ForestScan FBRMS plot. This was achieved using the  
720 [TreeQSM](#) software package (version 2.3; Raumonen et al., 2013), which [reconstructs](#) underlying woody surfaces [by fitting](#)  
721 [cylinders](#), as illustrated in Fig. 7. The QSM fitting process involves [three steps](#): (i) reducing each point cloud to a series of

**Deleted:** his modelling step

**Formatted:** Font: Italic

**Deleted:** 8

**Deleted:** 1

**Deleted:** 8

**Formatted:** Justified

**Deleted:** woody

**Deleted:** -level

**Deleted:** version 2.3

**Deleted:** employs cylinders to

**Formatted:** Font: Italic

**Deleted:** ,

**Deleted:** 9

**Deleted:** i

733 patches, (ii) analysing the spatial arrangement and neighbour relationships among patches, and (iii) robustly fitting cylinders  
734 to common patches.

735  
736 The overall QSM fit is controlled by three parameters, which are iterated into 125 different parameter sets, each generating  
737 five models. This yields a total of 625 candidate models per segmented tree. The optimal model is then selected by minimising  
738 the point-to-cylinder surface distance (Burt et al., 2019; Martin-Ducup et al., 2021). Estimates of morphological and  
739 topological traits such as volume, length, and surface area metrics, along with their mean and standard deviation, are derived  
740 from the five models that share the same parameters as the optimal model. This approach provides an estimate of the  
741 uncertainty associated with the resulting volume (Wilkes et al., 2023). In a HPC system, QSMs for a 1 ha plot can take up to  
742 2 days to complete.



745  
746 Figure 7: QSMs derived from individual tree-level point clouds acquired from plot LPG-01 in FBRMS-02: Lopé, Gabon.

Deleted: ii  
Deleted: assessing  
Deleted: between  
Deleted: iii  
Deleted: on  
Deleted: of the cylinders  
Deleted: results  
Deleted: in  
Deleted: potential  
Deleted: An  
Deleted: optimal  
Deleted: generated

Deleted: 9  
Deleted: the  
Deleted: shown in Fig. 8  
Deleted: .  
Formatted: Justified  
Deleted: ¶

765 Uncertainty estimates are reported for each ForestScan FBRMS plot and included alongside the final modelling outputs for  
766 every tree in a 'tree-attributes.csv' file, generated at the end of the modelling process. Sources of error in QSM fitting can arise  
767 from data acquisition (e.g., wind, leaf occlusion, understory vegetation) and from assumptions inherent in segmentation and  
768 fitting processes. Wilkes et al. (2017) discuss issues related to data acquisition and methodological choices, while Morhart et  
769 al. (2024) quantify their effects on branch size and volume under controlled conditions. Although these impacts are difficult  
770 to assess without reference (harvest) data, Demol et al. (2022) show that, where TLS and harvest data have been compared,  
771 agreement is generally within a few percent of AGB per tree. The report CVS file also includes tree- and plot-level carbon and  
772 AGB estimates, the latter based on a mean pantropical wood density value of 0.5 g cm<sup>-3</sup> derived from the DRYAD global  
773 database of tropical forest wood density (2009). Plot-level AGB was also estimated using DRYAD-derived regional mean  
774 wood densities and is presented in Table 5.

775 ▾  
776 Figures of all individually segmented trees arranged by tree DBH size (largest to smallest DBH) are also generated for each  
777 FBRMS plot, examples of which can be seen in Fig. 8. In a HPC system, tree figure for a 1 ha plot can take ~30 mins to  
778 complete. Figure 9 provides a comparison of the distribution of DBH measurements collected by tree census and TLS methods  
779 at each of the 10 ForestScan FBRMS 1 ha plots.

## 780 TLS datasets

781 The following terrestrial LiDAR-derived products are available for each of the 10 ForestScan FBRMS plots:

- 782 1. Raw terrestrial LiDAR data from each scan (no filtering was applied in RiSCAN PRO), stored in the RXP data stream  
783 format developed by RIEGL.
- 784 2. Transformation matrices necessary for rotating and translating the coordinate system of each scan, into the coordinate  
785 system of the first scan. Stored in DAT format.
- 786 3. Pre-processed terrestrial LiDAR data:
  - 787 a. full-resolution 10m tiled plot point clouds including attributes such as XYZ, scan position index, reflectance,  
788 deviation, etc. stored in polygon PLY format.
  - 789 b. downsampled 10m tiled plot point clouds including attributes such as XYZ, scan position index, reflectance,  
790 deviation, etc. stored in polygon PLY format.
  - 791 c. A tile\_index file (maps the spatial location of the tiled point clouds) stored in DAT format.
  - 792 d. Bounding geometry files setting plot boundaries with and without a buffer surrounding the plot. Stored in  
793 shapefile SHP, DBF, SHX and CPG formats.
- 794 4. Downsampled 10m tiled plot point clouds segmented into leaf, wood, ground points or coarse woody debris. Stored  
795 in polygon file format PLY format.
- 796 5. Wood-leaf separated tree-level point clouds including segmentation results and classification probabilities for each  
797 point are stored in polygon PLY format.

**Deleted:** The final modelling outputs for each tree are saved into a "tree-attributes.csv" report file, which is generated at the end of the modelling exercise. This file also includes tree and plot level carbon and AGB estimates, the last of which are based on a mean pantropical wood density value of 0.5 g/cm<sup>3</sup> estimated from the DRYAD global database of tropical forest wood density (Zanne et al., 2009). FBRMS plot AGB was also estimated using DRYAD-derived regional mean wood densities as shown in Table 4.¶

**Deleted:** 10

**Deleted:** 11

**Deleted:** diameter at breast height (

**Deleted:** )



849 files containing the GNSS scan position coordinates can be uploaded to Google Earth or read into a GIS tool such as QGIS  
 850 (QGIS Development Team, 2025; <https://qgis.org>)

851  
 852 **Table 5:** Summary statistics for 10 FBRMS ForestScan TLS plot datasets. AGB estimates use wood density values from the  
 853 DRYAD global database (Zanne et al., 2009): (1) *TLS2Trees* pantropical mean, (2) Tropical Africa mean (TAF, Gabon), (3)  
 854 South-East Asia mean (TS-EA, Malaysia), (4) Tropical South America mean (TSA, French Guiana), (5) Guyana community  
 855 mean (GF, French Guiana), and (6) allometric AGB estimates based on Chave et al. (2014).

Plot ID	Site	Census trees ( $\geq 10$ cm DBH)	TLS2trees plot summary				TLS2trees Carbon estimation			TLS2trees AGB estimations (1)			Tropical Africa (TAF; 2) / Tropical South America (TSA; 4) / Tropical South-East Asia (TS-EA; 3) AGB estimations			Guyana AGB estimations (5)			2014 Allometric AGB estimation (6)
			TLS trees (#)	TLS vs Census trees (%)	TLS plot area (ha)	TLS plot volume ( $m^3$ )	Plot C (t)	C per ha (t/ha)	Wood density ( $g/cm^3$ )	Plot AGB (t)	AGB per ha (t/ha)	Wood density ( $g/cm^3$ )	Plot AGB (t)	AGB per ha (t/ha)	Wood density ( $g/cm^3$ )	Plot AG B (t)	AGB per ha (t/ha)	Plot AGB (t)	
OKO-01	GA	388	397	2.58	1.08	829.05	195.24	181.60	0.5	414.52	385.57	0.60	495.77	459.05				378.62	
OKO-02	GA	472	473	0.21	1.02	625.45	147.29	143.97	0.5	312.72	305.67	0.60	374.02	366.69				351.35	
OKO-03	GA	339	355	4.72	1.04	959.59	225.98	218.19	0.5	479.79	463.26	0.60	573.83	551.76				372.82	
LPG-01	GA	340	275	-19.12	1.05	477.88	112.54	107.16	0.5	238.94	227.52	0.60	285.77	272.17				459.85	
FG5c_1	GF	1110	804	-27.57	1.06	529.67	124.74	117.62	0.5	264.83	249.73	0.63	334.75	315.80	0.73	386.66	409.86	327.30	
FG6c_2	GF	902	832	-7.76	1.10	751.13	176.89	161.48	0.5	375.57	342.86	0.63	474.72	431.56	0.73	548.33	603.16	421.90	
FG8c_4	GF	1116	1090	-2.33	1.09	625.80	147.38	135.76	0.5	312.90	288.24	0.63	395.50	362.85	0.73	456.83	497.95	286.10	
SEP-11	MY	584	659	12.84	1.05	961.36	226.40	214.67	0.5	480.68	455.78	0.57	551.82	579.41				499.91	
SEP-12	MY	469	380	-18.99	1.13	765.51	180.28	158.98	0.5	382.76	337.53	0.57	439.40	496.53				443.45	
SEP-30	MY	787	986	25.29	1.03	374.66	88.23	85.25	0.5	187.33	181.01	0.57	215.05	221.50				311.54	

**Deleted:** (Development, 2025b)(Team, 2025b)

**Formatted:** Font: (Default) +Headings (Times New Roman)

**Deleted:** ¶

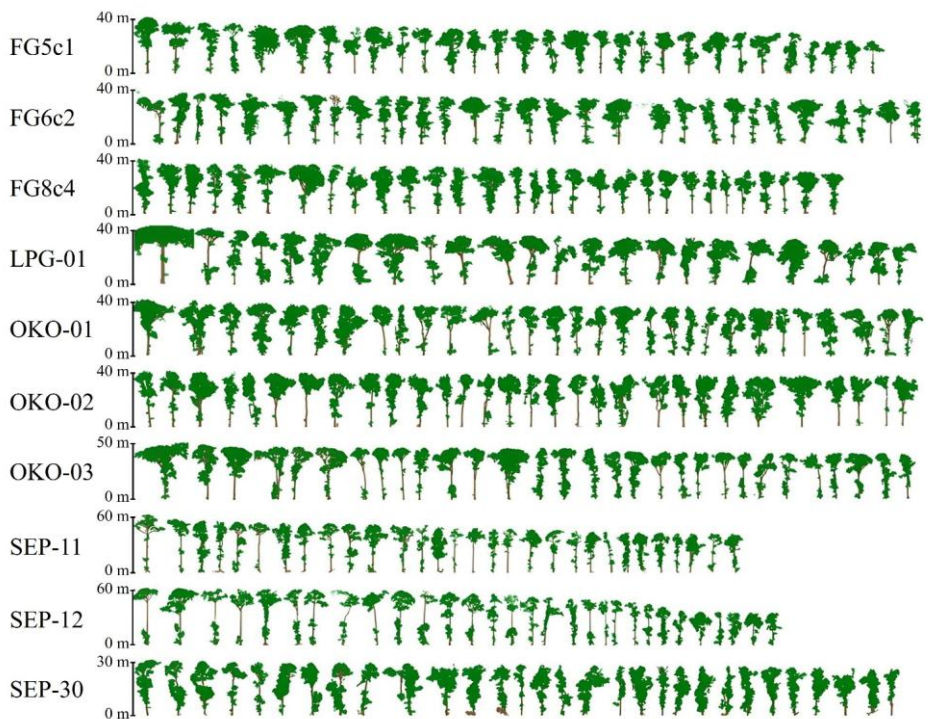
**Deleted:** 4

**Formatted:** Font: Italic

**Deleted:** Summary statistics for the 10 FBRMS ForestScan TLS plot datasets. AGB was estimated using different wood densities based on the DRYAD global database of tropical forest wood density (Zanne et al., 2009): 1) the *TLS2Trees* pantropical mean wood density, 2) a regional mean wood density for Tropical Africa (TAF) for our FBRMS plots in Gabon (GA), 3) a regional mean wood density for South-East Asia (TS-EA) for our FBRMS plots in Malaysia (MY), 4) a regional mean wood density for South America (TSA), 5) a Guyana community-mean wood density for FBRMS plots in French Guiana (GF), and 6) an allometric AGB estimates for all FBRMS plots based on Chave et al. (2014).

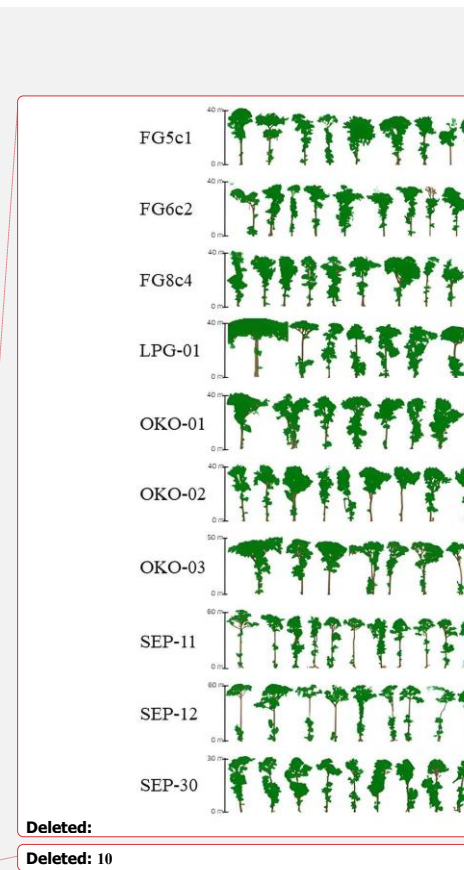
**Formatted Table**

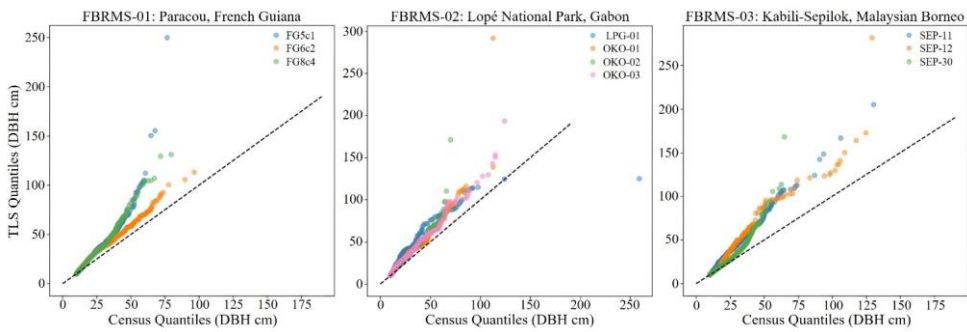
876



877

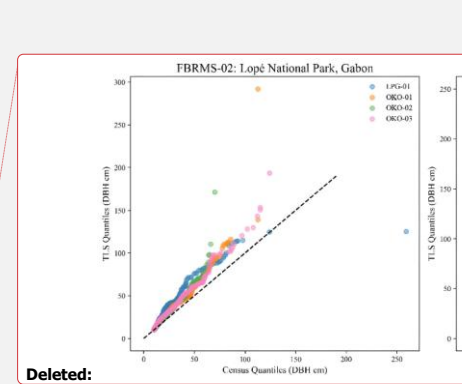
Figure 8: Examples of the largest trees (up to 30 trees) arranged in decreasing DBH size (1.3 m trunk height) for each of the 10 ForestScan FBRMS plots. The upper limit of the Y axis varies and ranges from 30 m to 60 m maximum tree size between plots.





883

884 **Figure 9:** Quantile-Quantile (QQ) plots comparing the distribution of DBH measurements collected by tree census and TLS  
 885 methods at each of the 10 ForestScan FBRMS 1 ha plots. TreeQSM measures DBH at the standard height of 1.3 m for each  
 886 TLS-extracted tree, whereas census DBH measurements are routinely adapted to account for tree buttresses found among  
 887 larger trees. Generally, census and TLS DBH measurements are in good agreement, **but consistently overestimated by TLS**.  
 888 Deviations for larger DBH values can be improved by adapting the DBH extraction of large buttressed trees once these trees  
 889 are matched to their census counterparts. The 1:1 reference line (dotted black line) represents perfect agreement between  
 890 census and TLS-extracted DBH measurements.



**Deleted:**

**Deleted:** 1

**Deleted:** diameter at breast height (

**Deleted:** )

**Deleted:** ;

**Deleted:** however, d

898 **2.2.3 Unpiloted Aerial Vehicle**Laser scanning (UAV-LS)

**Deleted:** AV-borne

899 Unlike TLS, there are currently no best practice guidelines for UAV-LS data acquisition for forest characterisation. Therefore,  
900 flight plans and parameters were implemented on a case-by-case basis, considering the site, instrument, sensor, and application.  
901 An important consideration in this respect is whether VLOS needs to be maintained, i.e., the visibility of the platform by the  
902 pilot throughout the mission. Regulations on this vary nationally and are changing rapidly as technology evolves and the use  
903 of UAVs expands. In Europe, for example, a risk-based approach has been introduced, allowing beyond VLOS, when risks are  
904 negligible.

**Deleted:** visual line of sight (

**Deleted:** )

**Deleted:** (BVLOS)

**Deleted:** Given the remote nature of the ForestScan FBRMSs, the likelihood of severe incidents involving non-crew persons is very low.

905  
906 Another important consideration is the availability of take-off and landing areas. Vertical take-off and landing (VTOL)  
907 platforms (e.g., quadcopters and octocopters) require smaller areas and are more flexible, while fixed-wing platforms may  
908 require substantial take-off and landing sites, although they offer greater area coverage and flight duration. The actual take-off  
909 area for VTOL platforms is highly dependent on the skills and confidence of the pilot. However, a very small take-off area  
910 surrounded by tree crowns typically also means low chances for VLOS operation, unless an above-canopy platform such as a  
911 cherry-picker is available.

912  
913 In the context of VTOL and VLOS operations, viewshed analysis based on already acquired ALS data has proved useful. ALS  
914 point clouds can be used to derive initial Digital Surface Models (DSM), which can identify possible take-off positions.  
915 Viewshed analysis can then use the DSM to simulate the visibility of the UAV from the take-off position.

916  
917 During data collection, attention should also be paid to acquiring access to GNSS observables from permanent base stations  
918 (e.g., CORS network) or to collecting observables with a temporary base station (e.g., Emlid Reach RS+ or RS2). A base  
919 station should be positioned less than 15 km from the survey area. For some platforms, Real-Time Kinematic (RTK), and  
920 therefore radio connection, between the UAV and base station can be an added constraint.

921  
922 Our UAV-LS data collections used three different LiDAR systems built by RIEGL at FBRMS-01 and FBRMS-02. All systems  
923 are based on the time-of-flight principle and capable of multi-return registration with the miniVUX-1DL being a specific  
924 downward-looking sensor designed for fixed-wing UAVs. Technical specifications for all three UAV-LS sensor systems are  
925 provided in Table 6.

926  
927 **Table 6:** UAV-LS sensor systems used at ForestScan FBRMS-01 and FBRMS-02.

Characteristic	miniVUX-1UAV	VUX-1UAV	miniVUX-1DL
Max Pulse Repetition Rate [kHz]	100	550	100

**Deleted:** Finally, the external framework for UAV operations comprises the legal regulations to operate UAVs, which are taught during pilot licence training. Consideration should be given to the legal issues involved in acquiring permission to use the airspace. Many aeronautical authorities have adopted the practice of regarding UAVs as regular airspace users comparable to crewed aircraft. In certain areas, this can have significant implications for planning, particularly regarding permissions that must be obtained and licences required by the pilots. Special attention should be paid to airports, as they are surrounded by controlled traffic regions (CTR). Flying within CTRs is only possible with special licences and equipment (transponder, radio). New technical developments are underway to equip UAVs with transponders, making CTR operations more feasible in the future. Additionally, military airspace (particularly relevant to FBRMS-01) requires thorough preparation and prior communication with the relevant authorities. Unlike civil airspace, low-flying exercises can be conducted in military airspace; however, the military has the right to completely block areas for exercises, even at short notice.¶

**Deleted:** 5

**Deleted:** below

**Deleted:** 5

Wavelength [nm]	905	1550	905
FOV [°]	360	330	46
Ranging accuracy / precision [mm]	15 / 10	10 / 5	15 / 10
Max range [m]	330 @ $\rho \geq 80\%$	1050 @ $\rho \geq 80\%$	260 @ $\rho \geq 80\%$
Weight [kg]	1.55	3.5	2.4
Inertial Measurement Unit (IMU)	Applanix APX20	Applanix AP20	Applanix APX15
Operated by	AMAP	Wageningen University	University of Edinburgh
Operated on	DJI M600	RiCOPTER	DELAIR DT26X
Flight location	FBRMS-01: Paracou	FBRMS-01: Paracou	FBRMS-02: Lopé
<u>Flights merged into single acquisition</u>	<u>No</u>	<u>No</u>	<u>Yes</u>

958

959 **UAV-LS: FBRMS-01: Paracou, French Guiana**

960 UAV-LS data was collected in October 2019 using two different scanning systems as shown in Tables 7 and 8. The first set  
 961 of 11 flights listed in Table 7 were conducted using the RIEGL VUX-1UAV mounted on a RIEGL RiCOPTER UAV and  
 962 flown over the same 200 x 200 m<sup>2</sup> area that was scanned with TLS covering subplots 2 and 4 in plot 6. Six of these flights  
 963 covered the entire 200 x 200 m<sup>2</sup> area with 20 m spacing between flight lines at an altitude of 120 m above ground level (AGL).  
 964 The remaining five flights covered only the north-east 100 x 100 m<sup>2</sup> area covering subplot 2 (i.e. FG6c2) with a criss-cross  
 965 pattern to maximise the diversity of viewing angles into the canopy. These latter flights were conducted at a lower altitude of  
 966 90 m AGL to increase point density; however, the entire plot could not be covered without losing VLOS.  
 967

**Deleted:** 5. As detailed

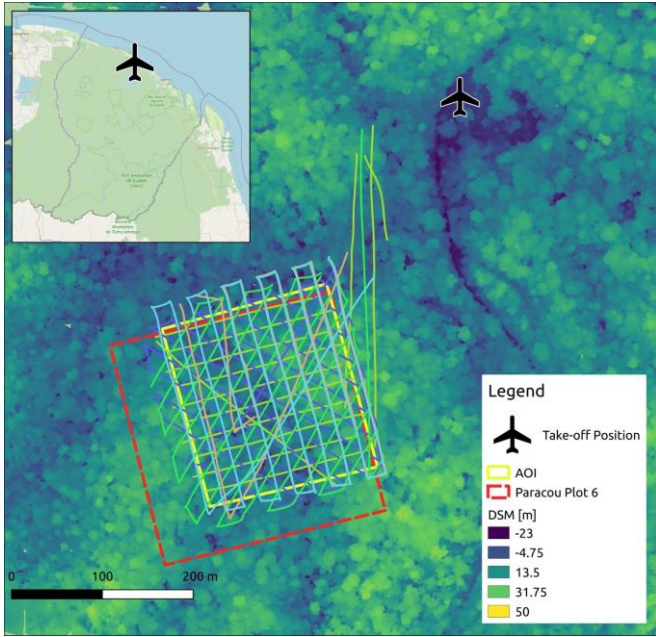
**Deleted:** in Fig. 12 and Table 6 below, a total of 11 flights

**Deleted:** sub-

**Deleted:** plot sub-

**Deleted:** visual line of sight (

**Deleted:** )



974  
975 **Figure 10:** UAV-LS flight trajectories over the FBRMS-01 site at Paracou, showing coverage of the experimental 4 ha plot 6  
976 (red dashed outline) and the area of interest (AOI; yellow dashed outline). The criss-cross flight pattern results from multiple  
977 flight lines oriented in different directions (e.g., N-S, E-W, NE-SW) to improve point density and reduce occlusion in dense  
978 tropical forest canopies. The background shows a digital surface model (DSM) with elevation values (m), colour-coded by  
979 elevation classes as indicated in the figure legend (-23 m to 50 m). The inset map shows the regional location of Paracou  
980 within French Guiana (© OpenStreetMap contributors, available at <https://www.openstreetmap.org>).  
981

982 **Table 7:** Overview of the 2019 VUX-1 UAV-LS flights at FBRMS-01 (Paracou), including plot ID, acquisition date/time,  
983 flight height above ground level (AGL), speed, and pulse repetition rate. Flight patterns refer to the orientation of flight lines:  
984 N-S (north-south), E-W (east-west), NE-SW (northeast-southwest), and “criss-cross” indicates multiple orientations flown  
985 over the same area as seen in Fig. 10. All flights listed can be considered part of one acquisition and are provided as individual  
986 point clouds in this dataset. Users may merge them according to their needs.▼

Plot ID	Date & Time (UTC ISO 8601)	Direction [°]	Interline [m]	Alt	Speed [m/s]	Pulse Repetition Rate [kHz]
---------	----------------------------	---------------	---------------	-----	-------------	-----------------------------

**Deleted:** 2

**Formatted:** Justified, Right: 0 cm, Space After: 0 pt, Line spacing: 1.5 lines

**Deleted:** Font: Not Bold

**Deleted:** Font: (Default) Times New Roman, Not Bold

**Deleted:** Font: Not Bold

**Deleted:** Font: Not Bold

**Deleted:** UAV-LS acquisitions over FBRMS-01: Paracou with flight trajectories covering ForestScan plot FG6c2. Inset map data © OpenStreetMap contributors, available from <https://www.openstreetmap.org>.▼

**Deleted:** 6

**Formatted:** Font: (Default) +Body (Times New Roman)

**Deleted:** Font: (Default) +Body (Times New Roman)

**Deleted:** Overview of 2019 VUX-1 UAV-LS flights in FBRMS-01: Paracou. Flight pattern N-S = flight in lines oriented from North to South, etc. and criss-cross = multiple flight directions.

**Deleted:** Flight pattern

**Deleted:** Height

**Deleted:** Velocity

**Formatted Table**

				AGL [m]		
P6 200	<u>2019-10-18T11:41:05Z</u>	Manual	<u>20</u>	115	4	550
P6 200	<u>2019-10-18T13:28:27Z</u>	<u>165</u>	<u>20</u>	110	6	550
P6 200	<u>2019-10-18T14:36:54Z</u>	<u>75</u>	<u>20</u>	105	7	550
P6 200	<u>2019-10-18T175:7:53Z</u>	<u>120</u>	<u>20</u>	115	6	550
P6 200	<u>2019-10-18T19:23:14Z</u>	<u>30</u>	<u>20</u>	105	6	550
P6 200	<u>2019-10-19T16:34:12Z</u>	<u>165</u>	<u>20</u>	120	6	300
P6 200	<u>2019-10-20T18:45:40Z</u>	<u>165</u>	<u>20</u>	120	6	100
P6 100	<u>2019-10-19T12:10:41Z</u>	<u>multiple headings</u>	<u>variable</u>	95	4	550
P6 100	<u>2019-10-19T12:41:09Z</u>	<u>multiple headings</u>	<u>variable</u>	85	4	550
P6 100	<u>2019-10-19T18:19:57Z</u>	<u>multiple headings</u>	<u>variable</u>	95	4	550
P6 100	<u>2019-10-19T19:41:42Z</u>	<u>multiple headings</u>	<u>variable</u>	90	4	550

999

1000 UAV-LS data was also collected over several plots using a different UAV-LS system -a YellowScan Vx20 containing a RIEGL  
 1001 Mini-VUX scanner and Applanix 20 IMU- mounted on a DJI M600. Details for a second set of 12 flights can be found in  
 1002 Table 8. To allow for comparisons with the VUX system, coincident acquisitions were performed over experimental plot 6  
 1003 (covering all four subplots) and several others within the Paracou Research Site (see Table 8). A full description of the UAV-  
 1004 LS data collection for this UAV-LS data is provided in Brede et al. (2022b).

1005  
 1006 **Table 8:** Overview of UAV-LS flights using a YellowScan Vx20 system (RIEGL Mini-VUX scanner and Applanix 20 IMU)  
 1007 mounted on a DJI M600 during the 2019 mission at the FBRMS-01 site. Automated flight plans were performed using flight  
 1008 plans with the UgCS route planning software in grid mode. The table lists plot ID, acquisition date/time, flight parameters  
 1009 (direction, interline spacing, altitude and speed). Altitude values are reported as specified during flight planning with some  
 1010 missions using Above Ground Level (AGL), while others used Above Mean Sea Level (AMSL) due to differences in mission  
 1011 planning and operational requirements. These original specifications are retained to accurately reflect acquisition parameters.  
 1012 Pulse repetition for the RIEGL Mini-VUX scanner is fixed at 100kHz. Flights cover multiple experimental plots: 4 & 5 (single  
 1013 flight), 6 (8 flights), 7, 8, 10, 15, and the Tower plot (two flights) within the Paracou Research Site. All listed flights are  
 1014 provided individually; users may merge flights covering the same plot if needed for analysis.

**Deleted:** ¶**Deleted:** \_**Deleted:** \_**Deleted:** N-S**Deleted:** \_**Deleted:** E-W**Deleted:** \_**Deleted:** NW-SE**Deleted:** \_**Deleted:** NE-SW**Deleted:** \_**Deleted:** N-S**Deleted:** \_**Deleted:** N-S**Deleted:** \_**Deleted:** criss-cross**Deleted:** \_**Deleted:** criss-cross**Deleted:** \_**Deleted:** criss-cross**Deleted:** \_**Deleted:** criss-cross**Deleted:** \_**Deleted:** during the same mission as that using the RiCOPTER but  
 Deleted: separate**Deleted:** Scanning was performed using automated flight plans with the UgCS route planning software in grid mode.**Deleted:** Flight d**Deleted:** 7**Deleted:** below**Deleted:** Plot**Deleted:** 6,**Deleted:** Arbocel (a few kilometres west of the Paracou site and covering ForestScan plot FG6c2), and the Plantation area (500 metres north of the Paracou site)**Deleted:** The two sites acquired outside of Paracou correspond to contrasting vegetation: young secondary forest for Arbocel and plantations, for which field data can be obtained.**Deleted:** FBRMS**Deleted:** 7**Deleted:** Overview of miniVUX UAV-LS flights in FBRMS-01 Paracou.**Formatted:** Font: Bold

Plot ID	Date & Time (UTC)	Direction [°]	Interline [m]	Alt [m]	Speed [m/s]	Pulse Repetition Rate [kHz]
P4 & P5	2019-10-19T17:23:47Z	345	50	100 amsl	5	100
P6	2019-10-18T12:40:06Z	345	20	80 AGL	5	100
P6	2019-10-18T13:10:43Z	345	20	80 AGL	5	100
P6	2019-10-18T18:30:57Z	120	20	80 AGL	5	100
P6	2019-10-18T18:54:16Z	120	20	80 AGL	5	100
P6	2019-10-18T20:09:32Z	165	20	145 amsl	5	100
P6	2019-10-19T11:59:17Z	75	20	145 amsl	5	100
P6	2019-10-19T19:03:45Z	75	20	80 AGL	5	100
P6	2019-10-20T19:17:57Z	345	40	100 amsl	3	100
P8	2019-10-20T11:39:07Z	75 & 345	50	105 amsl	5	100
P GuyaFlux tower/CNES (tropiscat)	2019-10-19T16:25:57Z	0	50	80 AGL	5	100
P GuyaFlux tower/CNES (tropiscat)	2019-10-19T18:10:21Z	90	50	105 amsl	5	100

1056

## 1057 UAV-LS data processing

1058 All collected raw data underwent processing with standard tools. For VUX-1UAV data, this included processing  
 1059 recorded global navigation satellite system (GNSS) and base station data to flight trajectories with POSPac Mobile  
 1060 Mapping Suite 8.3 (Applanix, Richmond Hill, Ontario, Canada), laser waveform processing to discrete returns and geolocation  
 1061 in world coordinates with RIEGL RiProcess 1.8.6. For miniVUX-1UAV, waveform processing is performed online in the  
 1062 sensor. Point cloud processing and geolocation was performed with the CloudStation software (Yellowscan, Montpellier,  
 1063 France), using the Strip Adjustment option. For all UAV-LS data, only points with a reflectance larger than -20 dB were kept  
 1064 for further processing. Points with reflectance smaller than -20 dB consist mainly of spurious points caused by water droplets  
 1065 under high humidity conditions (Schneider et al., 2019).

Formatted Table
Deleted: Alt
Deleted: Arbocel
Deleted: Paracou
Deleted: P
Deleted: YS-
Deleted: -
Deleted: 80 AGL
Deleted: Paracou
Deleted: P
Deleted: YS-
Deleted: -
Deleted: 80 AGL
Deleted: Paracou
Deleted: P
Deleted: YS-
Deleted: -
Deleted: 80 AGL
Deleted: Paracou
Deleted: P
Deleted: YS-
Deleted: -
Deleted: 80 AGL
Deleted: Paracou
Deleted: P
Deleted: YS-
Deleted: -
Deleted: 80 AGL
Deleted: Paracou
Deleted: P
Deleted: YS-
Deleted: -
Deleted: 80 AGL
Deleted: Paracou
Deleted: P
Deleted: YS-
Deleted: -
Deleted: 145 amsl
Deleted: Paracou
Deleted: P
Deleted: YS-
Deleted: -
Deleted: 145 amsl
Deleted: Paracou
Deleted: P
Deleted: YS-
Deleted: -
Deleted: 100 amsl
Deleted: Paracou P7
Deleted: P
Deleted: YS-

1185  
1186 LiDAR point clouds were processed using the *LAStools* suite (rapidlasso GmbH). First, a 1-m resolution digital surface model (DSM)  
1187 was generated with **lasgrid** using the highest return within each cell. Ground points were then classified  
1188 with **lasground** (wilderness settings, 15-m step), and a 1-m digital terrain model (DTM) was derived from ground-classified  
1189 points using **las2dem**. Heights were normalized by subtracting ground elevation with **lasheight**, producing a set of height-  
1190 normalized point clouds. A 1-m canopy height model (CHM) was computed with **lascanopy**, retaining the maximum height  
1191 in each grid cell after removing noise and low-confidence classes. Finally, a point density map (1-m resolution) was created  
1192 using **lasgrid** with the *counter* option. This workflow produced consistent DSM, DTM, CHM, and density layers suitable for  
1193 subsequent ecological analyses. These UAV-LS datasets are freely available via the Centre for Environmental Data Analysis  
1194 (CEDA) with DOIs provided in section 5. Data access.

**Formatted:** Justified, Line spacing: 1.5 lines

#### 1195 UAV-LS: FBRMS-02: Lopé, Gabon

1196 UAV-LS data was collected in June 2022, concurrently with TLS data acquisition at this FBRMS. Data was acquired using a  
1197 DELAIR DT26X [drone platform](#) equipped with a RIEGL miniVUX-1DL (Mcnicol et al., 2021) as seen in Fig. 11. This  
1198 platform differs from the one used at FBRMS-01: Paracou in that it is designed for large-scale data acquisitions (thousands of  
1199 hectares) and is capable of operating beyond the VLOS, with an average flight speed of 17 m/s (61 km/h). Flights were  
1200 conducted in perpendicular lines at a nominal altitude of 120 m above the ground surface, with an average flight line spacing  
1201 of 20 m (based on 70–80% overlap). Each one-hour flight covered approximately 120–200 hectares with an estimated point  
1202 density of 400 points per square metre. To obtain the required densities, several flights were conducted over the core plots  
1203 from different angles (depending on wind conditions) to maximise the diversity of viewing angles into the canopy.

**Deleted:** Trajectometry was post-processed in POSPac UAV (V8.3) using single station DGPS corrections from a local SXBlue base station or the Kourou IGN network. Raw LAS points were exported using the YellowScan CloudStation software with the ‘line adjustment’ option. Further improvement of inter-line matching was performed using BayesMap software to account for an undetected defect in roll angle recording on the scanner unit. Merging and processing of each flight were conducted with LAStools software ([https://github.com/LAStools/LAStools\\_v1.0-1.4](https://github.com/LAStools/LAStools_v1.0-1.4)) for point cloud classification using the ‘*lasground*’ function with the options ‘-step 15°’ and ‘-wilderness’, and for the generation of DTM, DSM, and CHM at 1 m resolution. This UAV-LS dataset is freely available via the Centre for Environmental Data Analysis (CEDA) with DOIs provided in section 4. Data access.

**Deleted:** ure

**Deleted:** 3 below



**Deleted:** 3

**Deleted:**

**Deleted:** (i)

**Deleted:** )

1221

1222 **Figure 11:** UAV-LS acquisitions at FBRMS-02: Lopé using a fixed-wing system. This UAV employs a conventional take-off  
 1223 and landing (CTOL) procedure, with launch aided by a catapult (top). Once airborne, the UAV is controlled from a laptop  
 1224 connected to the UAV via an antenna (middle). The flight trajectory is corrected to centimetre precision using data collected  
 1225 from a static GNSS receiver placed within 10 km of the UAV operating area (lower left). Additional refinements and  
 1226 corrections are possible via ground control points located across the study area (lower middle), the positions of which are  
 1227 measured using a 'rover' GNSS receiver (lower right). Image originally published in McNicol et al. (2021).

1233 **UAV-LS data processing**

1234 Flight trajectories were reconstructed using GNSS/IMU measurements and adjusted with differentially corrected base station  
 1235 data in Applanix POSPac software. The corrected flight paths and laser data were then integrated using the RIEGL software  
 1236 package, RiPROCESS, to generate the initial three-dimensional point cloud. Residual trajectory errors—such as discrepancies  
 1237 in GPS tracking and elevation—were corrected by using small buildings as reference points to refine the relative position and  
 1238 orientation of individual flight lines and scans. Further adjustments were made using ground control points: square targets (1–  
 1239 2 m<sup>2</sup>) composed of alternating black and white material arranged in a checkerboard pattern. This process resulted in a LiDAR-  
 1240 derived point cloud with a geometric accuracy of 1.8 cm. All elevation data were calculated as ellipsoidal heights (m) within  
 1241 the UTM 32S coordinate system. Each flight was processed separately, and all datasets were merged prior to export.  
 1242 Subsequent point cloud processing was carried out using elements of the lidR package (v3.1.0; Roussel et al., 2020). This

1243 UAV-LS dataset is freely available via the Centre for Environmental Data Analysis (CEDA) with DOIs provided in section 5.  
 1244 Data acquisition characteristics can be found in Table 6.

1245  
 1246 **Table 9:** Comparison of ALS acquisition characteristics for two ForestScan sites: FBRMS-01:Paracou, French Guiana and  
 1247 FBRMS-03: Kibili-Sepilok, Malaysian Borneo. These key flight and sensor characteristics can support alignment and  
 1248 comparability across sites.

ALS flight characteristics	FBRMS-01: Paracou, French Guiana	FBRMS-02: Kibili-Sepilok, Malaysian Borneo
Date	Nov 2019	Feb 2020
Area covered	10 km <sup>2</sup>	27 km <sup>2</sup> (Kibili-Sepilok) + 20 km <sup>2</sup> (Danum Valley protected area) + 9 km <sup>2</sup> (reduced impact logging area adjacent to Danum Valley)
Scanner	RIEGL LMS - Q780	RIEGL LMS - Q560
Platform	BN2 aircraft	Helicopter
Altitude	~900 m	~350 m (above forest canopy)
Speed	~180 km/h (50 m·s <sup>-1</sup> )	~100 km/h (30 m·s <sup>-1</sup> )
Scan angle	±30°	±30°
Pulse density	Min 15 pts/m <sup>2</sup> ; Mean 40 pts/m <sup>2</sup>	Mean 40 pts/m <sup>2</sup>
Overlap	80%	40%
CRS	EPSG:2972	EPSG: 32650

Deleted: (Adams et al., 2025)

Deleted: UAV-LS data processing commences with the post-processing of the platform's trajectory based on GNSS observations (rover) in conjunction with the Inertial Measurement Unit (IMU) and Global Navigation Satellite System (GNSS) observables from a base station, i.e., Post Processed Kinematic (PPK) processing (Brede et al., 2017). LiDAR waveforms must be interpreted to produce discrete returns in the scanner's own coordinate system. The post-processed trajectory can then be combined with the ranging information to generate point clouds in a global coordinate system. This processing pathway ensures global registration of the point clouds with survey-grade accuracy in the best-case scenario. If necessary, flight lines can be further fine-registered based on point cloud features, typically using automatic feature finding similar to RIEGL's Multi-station Adjustment (MSA) routine for TLS. Software packages for processing are usually provided or offered by the vendor of the UAV-LS system. The end product of this process is the globally registered point cloud.¶

¶ The point cloud can be treated as an ALS point cloud, allowing the application of standard processing steps such as ground point detection, DEM/DSM/CHM generation, and individual tree detection. The final step of tree detection remains an ongoing development because UAV-LS has a much higher point density than ALS but typically cannot detect trunks as clearly as TLS (Chen et al., 2021; Terryn et al., 2022; Torresan et al., 2020; Yan et al., 2020).

Deleted: 4. Data access

Formatted: Left

Formatted Table

1277 **2.2.4 Airborne Laser Scanning (ALS)**

1278 **FBRMS-01: Paracou, French Guiana**

1279 ~~ALS data were acquired~~ over Paracou in November 2019. The data covers 10 km<sup>2</sup>, including all ~~experimental~~ plots and areas  
1280 covered by ~~TLS~~ and ~~UAV-LS~~ (see Fig. 1). During the same campaign, additional data was gathered over Nouragues Research  
1281 Station in French Guiana. This supplementary data was collected using identical scanning ~~characteristics (provided in Table~~  
1282 9) and has been incorporated into the ForestScan data archive.

1283 ~~ALS~~ data for Paracou are freely available via the Centre for Environmental Data Analysis (CEDA) with DOIs provided in  
1284 section 5. Canopy height models for both Paracou and Sepilok are described in Jackson *et al.* (2024) and available at  
1285 <https://doi.org/10.908679>.

1287 **FBRMS-03: Kabilis-Sepilok, Malaysia**

1288 ~~ALS data were acquired at Kabilis-Sepilok~~ in February 2020. This dataset includes LiDAR and RedGreenBlue (RGB) imagery  
1289 ~~data collected from a helicopter over the Kabilis-Sepilok Forest Reserve and an additional non-ForestScan site – Danum Valley~~  
1290 ~~Forest Reserve~~. These areas were selected due to the availability of prior ~~ALS~~ data collected in 2013 and 2014. The complete  
1291 collection and processing details for these datasets are detailed in Jackson *et al.* (2024).

1292 The point cloud data for this FBRMS are available in LAS (LASer) format, as well as RGB data summary rasters in .tif format.  
1293 The raster images were processed with LAStools using default parameters. Canopy Height Model (CHM), Digital Surface  
1294 Model (DSM), Digital Terrain Model (DTM), and pulse density (pd) data are also included. The RGB data are provided in  
1295 jpg format and organised by flight date. The data was georeferenced using ground control points. This ~~ALS~~ dataset is freely  
1296 available via the Centre for Environmental Data Analysis (CEDA) with DOIs provided in section 5.

1298 **3. Recommendations for aligning and matching datasets**

1299 We provide data that are internally consistent in terms of pre-processing, geo-referencing, and exported in formats compatible  
1300 with open-source tools. Any further processing will depend largely on the intended application, such as individual tree analysis  
1301 or plot-level studies.

1302 For TLS data, all point clouds within a single plot are co-registered into one unified point cloud. These are subsequently  
1303 processed into individual tree point clouds, to which quantitative structural models (QSMs) are fitted to estimate volume.  
1304 Datasets for FBRMS-01 and FBRMS-02 were acquired using a RIEGL VZ-400i equipped with GNSS RTK positioning.

<b>Deleted:</b> Airborne laser scanning (
<b>Deleted:</b> )
<b>Deleted:</b> was collected
<b>Deleted:</b> field
<b>Deleted:</b> terrestrial laser scanning (
<b>Deleted:</b> )
<b>Deleted:</b> unmanned aerial vehicle LiDAR scanning (
<b>Deleted:</b> )
<b>Deleted:</b> . The data collection was conducted by the private company Altoa using a BN2 aircraft flying at approximately 900 m altitude at a speed of approximately 180 km/hr (that is, 50 m.s <sup>-1</sup> ). The LiDAR instrument used was a RIEGL LMS-Q780, with a minimum pulse density of 15 points/m <sup>2</sup> and a mean pulse density of 40 points/m <sup>2</sup> . The lateral overlap between two flight lines was 80%, with a scan angle of +/- 30 degrees.
<b>Deleted:</b> parameters
<b>Deleted:</b> Airborne LiDAR point cloud
<b>Deleted:</b>
<b>Deleted:</b> provided in a local coordinate reference system (EPSG:2972) and
<b>Deleted:</b> 4. Data access
<b>Moved (insertion) [3]</b>
<b>Deleted:</b> The collection and processing of
<b>Deleted:</b> for
<b>Deleted:</b> this FBRMS
<b>Deleted:</b> are detailed in Jackson <i>et al.</i> (2024)
<b>Deleted:</b> . The data was collected
<b>Deleted:</b> by Ground Data Solutions using a RIEGL LMS-Q560 scanner with a scanning angle of +/- 30 degrees from a helicopter flying at an altitude of 350 m above the forest canopy and at a speed of approximately 100 km/h (ca. 30 m.s <sup>-1</sup> ).
<b>Deleted:</b> two forest sites in Sabah, Malaysia
<b>Deleted:</b> , in February 2020. The 27 square kilometres covered by
<b>Deleted:</b> Reserve were fully scanned on 15 February 2020. In the
<b>Deleted:</b> , scanning between 19 and 22 February, 2020 covered two adjacent areas: a protected zone (20 square kilometres) and a reduced impact logging zone (9 square kilometres)
<b>Deleted:</b> airborne LiDAR
<b>Moved up [3]:</b> This dataset includes LiDAR and RedGreenBlue (RGB) imagery data collected from a helicopter over two forest sites
<b>Deleted:</b> have approximately 42 pulses per square metre and
<b>Deleted:</b> and provided in the 'WGS 84 / UTM 50N' coordinate
<b>Deleted:</b> UAV-
<b>Deleted:</b> 4. Data access
<b>Deleted:</b> A

1361 However, as GNSS performance is often compromised beneath dense tropical canopies, positional accuracy for these datasets  
1362 should be interpreted with caution.

1363  
1364 UAV-LS and ALS datasets are geo-referenced in each case. As positional accuracy depends on the IMU and GNSS  
1365 measurements, which can introduce errors manifesting as height biases between individual flightlines. Although we did not  
1366 observe such discrepancies in our data, a rigorous comparison with ground control points would be required to confirm this  
1367 definitively -a step we have not undertaken. These datasets have not been explicitly aligned or matched to one another.  
1368 Alignment can be performed, but it requires manual identification of control points in each dataset and, as noted above, will  
1369 depend on the intended use of the resulting data.

### 1370 **3.1 Matching TLS to census data: stem maps**

1371 A key step in estimating AGB from tree-level terrestrial laser scanning (TLS) point clouds is the selection of wood density for  
1372 converting volume to mass. Wood density, represents a significant source of uncertainty in the indirect estimation of AGB,  
1373 whether through allometry and census DBH, EO-derived canopy height, TLS-estimated volume, or other methods (Phillips et  
1374 al., 2019). If the censused trees in each plot can be matched to their TLS counterparts, literature estimates of species-specific  
1375 WD (or field-measured values, if available) can be used. In the absence of such a match, plot-level mean WD values are  
1376 employed, as is common in most EO-derived estimates that rely on large-scale allometric models (e.g. Chave et al., 2014).  
1377 Research by Momo et al. (2020), Burt et al. (2020), and Demol et al. (2021) has demonstrated that significant bias can occur  
1378 in TLS-derived AGB estimates due to within-tree WD variations when literature-derived species average WD values are used.  
1379 However, Momo et al. (2020) suggest there is sufficient correlation between vertical gradients and basal WD to allow for  
1380 empirical corrections.

1381 While it is preferable to match TLS trees to census trees, this process is not straightforward and is currently only possible  
1382 manually (if at all) after TLS data acquisition and co-registration. Once registered, a slice through the TLS plot-level point  
1383 cloud can be generated, enabling the identification of individual trees from their stem profiles. This stem map can be provided  
1384 in hard copy or digital format (e.g., high-resolution PDF) to the census team, who can then revisit the plot, moving through it  
1385 in the same manner as during the census—starting at the plot’s southeast corner or 0,0 and moving up and down by 10 m  
1386 quadrants—annotating the TLS stem map with each tree census ID. This process can be conducted separately or as part of an  
1387 existing census but is best performed simultaneously or as soon as possible after TLS collection to minimise changes and  
1388 facilitate collaboration between TLS and census teams. Despite success with this approach in some plots (e.g., Gabon 2016),  
1389 experience has shown that significant understory, terrain variation, and/or changes and tree falls between census and TLS data  
1390 collection (e.g., ~2 years between census and TLS data collection for FBRMS-03 plots, and significant tree falls and changes  
1391 due to a storm between census and TLS data collection in FBRMS plot LPG-01 in Gabon) make this process very challenging,  
1392 particularly for smaller stems (in the 10-20 cm DBH range).

**Deleted: 1**

**Deleted:** above-ground biomass (

**Deleted:** )

**Deleted:** (WD)

**Deleted:** D

**Deleted:** diameter at breast height

**Deleted:** (

**Deleted:** )

**Deleted:** Earth observation (

**Deleted:** )

1404 **3.2 Aligning TLS to UAV-LS data (and other spatial data)**

1405 Through its accurate global registration via PPK processing, UAV-LS can be regarded as a high-quality geometric reference  
1406 for registration. For the purpose of comparison with accurate ALS data or satellite observations, a registration of TLS to the  
1407 UAV-LS point cloud is highly recommended. The integration of GNSS directly into TLS data collection now ensures that  
1408 registered plot-level point clouds are aligned within a global coordinate system. This significantly facilitates the co-registration  
1409 of TLS and UAV-LS point clouds, given that GNSS accuracy is typically within 1 metre. Historically, placing all LiDAR point  
1410 clouds within accurate global coordinate systems necessitated dedicated survey measurements of plot corners or TLS locations  
1411 via GNSS, a process often hindered by signal attenuation in dense forests. Consequently, GNSS surveying of plot corner  
1412 locations is not a standard component of forest census protocols, although it should be considered essential for plots intended  
1413 for EO calibration and validation purposes. The reduced cost of RTK GNSS equipment and its subsequent routine integration  
1414 into TLS workflows have made this more feasible, despite the challenges in obtaining fixed positions, and maintaining radio  
1415 link with a base positioned on a well-known point under deep forest canopy cover. While this may not benefit ALS directly,  
1416 UAV-LS is likely to serve as a valuable intermediary between TLS (and census data) and ALS. The requirement for global  
1417 GNSS positioning also extends to other spatial datasets.

1418 **3.3 Aligning TLS and UAV-LS to ALS data**

1419 Aligning ALS data with TLS and UAV-LS datasets presents significant challenges. Despite the use of high-quality GNSS  
1420 positioning, meter-scale geolocation discrepancies between sensors can occur. Co-locating LiDAR datasets acquired at  
1421 different scales -TLS, UAV-LS, and ALS- remains complex, with no standard or “turn-key” solution currently available.  
1422 Manual intervention is often required, and the approach varies by site and sensor combination. While plot-level AGB  
1423 estimation is relatively tolerant to these discrepancies, finer-scale applications (e.g., matching to tree-level census data) demand  
1424 more precise alignment. This can be partially addressed through manual co-registration using common tie points across  
1425 datasets.

1426 Formatted: Normal

1427 Achieving meaningful alignment also depends on the internal characteristics of ALS point clouds. Acquisition parameters such  
1428 as point density, scan angle distribution, and footprint size influence comparability and should be controlled as far as possible.  
1429 Post-processing can regularise point density and scan angles within or across campaigns, improving consistency.  
1430 Homogeneous scanning geometry enables more stable structural metrics and enhances AGB prediction performance.  
1431 Similarly, parameters such as transmitted pulse power (which co-varies with pulse repetition rate) and flight altitude (affecting  
1432 footprint size and canopy penetration) should be standardised across acquisitions to minimise bias (Vincent et al., 2023). These  
1433 steps are critical for reducing alignment errors and ensuring robust comparisons between TLS, UAV-LS, and ALS datasets.

#### 1434 4. Recommendations for data collection in FBRMS

1435 Building on this first case study, we make the following general recommendations for data collection of tropical forest plot  
1436 census, TLS, UAV-LS and ALS data for the specific application of estimating AGB and upscaling to ~~EQ~~ estimates. These  
1437 recommendations follow from the CEOS LPV AGB protocol and subsequent requirements identified for the GEO-TREES  
1438 initiative.

1439 • **Consistent data acquisition and processing:** in order to facilitate the comparison of AGB estimates between sites,  
1440 dates, teams, etc. care should be taken to collect and process data as consistently as possible. This ~~might seem~~ obvious  
1441 but is particularly important as the use of TLS and UAV-LS for AGB estimation (and even ALS in some cases) are  
1442 currently primarily research-led (as opposed to fully operational). As new methods and tools are developed, including  
1443 newer versions of existing software, care should be taken to ensure backwards compatibility of the resulting AGB  
1444 estimates. This means either re-processing older data, or at the very least, some form of cross-comparison of original  
1445 and new methods. In our experience, listed below are some of the areas where care is needed to ensure data  
1446 consistency and reduce bias and uncertainty:

1447 • **TLS data acquisition** - comparison between sites and plots is made much easier by using the same census,  
1448 TLS, UAV-LS and ALS data acquisition and processing protocols. Even within the forest plot census  
1449 community there are slightly different protocols and processes between different plot networks. This is even  
1450 more variable for different ~~sources~~ of LiDAR data. We note that much of the TLS work in tropical forests  
1451 aimed at volume reconstruction and AGB estimation has been carried out with RIEGL VZ series TLS  
1452 instruments. We make no comment as to what is 'the best' instrument - there are various cost/benefit trade-  
1453 offs to be made. Equipment has to be robust to withstand tropical forest work (and humidity). LiDAR range  
1454 needs to be in the 100s of metres to ensure points are returned from tall canopies. Phase-shift TLS systems  
1455 can be light and have very rapid scan rates, but suffer from 'ghosting' of multiple returned hits along a beam  
1456 path. Mobile Laser Scanning (MLS) systems offer rapid coverage, and require minimal input for registration  
1457 by using simultaneous location and mapping (SLAM), but tend to have lower range and precision due to the  
1458 uncertainty in absolute location resulting from SLAM. It is likely that these systems will become more  
1459 powerful and precise, offering a possible alternative to static tripod-mounted TLS in the future for AGB  
1460 applications. Specific issues to consider are TLS power. For example, the RIEGL VZ-400 and newer VZ-  
1461 400i systems (both used here) have different recording sensitivities i.e. down to -30 dB for the newer VZ-  
1462 400i, whereas the VZ-400 only recorded to -20 dB. This can have a significant impact on the number of  
1463 returns, particularly from further away and higher in the canopy and should be taken into consideration when  
1464 comparing results between older and newer TLS instruments. Choices are also possible in terms of power  
1465 settings: lower power settings reduce scan times & extend battery time, but also significantly reduce the

**Deleted:** ALS presents another challenge; despite the use of high-quality GNSS, m-scale geolocation discrepancies with UAV-LS and TLS data may still occur. The co-location of LiDAR datasets from different sensors and at varying scales -TLS, UAV-LS, and ALS- remains challenging, with no standard or 'turn-key' solution available. Manual intervention and processing are often required, varying for each site and sensor combination. For plot-level estimation of above-ground biomass (AGB), co-location is less critical, but at finer scales (e.g., for matching to tree-scale census data), this issue can potentially be mitigated through manual co-registration by identifying common tie points.¶

ALS point cloud characteristics depend on various acquisition parameters that should be controlled as much as possible. Point density, point density regularity, and scan angles may be regularised within or across campaigns during post-processing. Homogeneous scanning density and scanning angles enable the extraction of more stable statistics from the point clouds, thereby improving AGB prediction performance. To meaningfully compare point clouds across different sites or dates, other parameters should be kept constant as far as possible. These include the pulse transmitted power (which typically co-varies with Pulse Repetition Rate) and the flight altitude (which affects pulse irradiance and footprint size, and consequently, LiDAR pulse penetration) (Vincent et al., 2023).¶

**Deleted:** arth

**Deleted:** bservation

**Deleted:** ay sound

**Deleted:** types

1494 quality of resulting point clouds, particularly higher in the canopy. TLS data were collected using a pulse  
1495 repetition rate (PRR) of 300 kHz on RIEGL VZ-400 and VZ-400i scanners, trading longer scan times for a  
1496 fixed angular resolution to maximise coverage at the tops of tall trees. In the RIEGL configuration, PRR and  
1497 emitted laser power are intrinsically linked: increasing the PRR reduces the available power, and vice versa.  
1498 Consequently, the choice of PRR determines the power setting, and adjustments to one parameter necessarily  
1499 influence the other. However, recent work by Verheltz et al. (2024) suggests that using lower power, but  
1500 with higher angular resolution, can achieve better coverage in tall forests for the same scan duration (3 mins  
1501 per scan). More generally, comparing measurements made with scanners of varying power, sensitivity,  
1502 resolution etc. will compound uncertainties (particularly biases) in the resulting estimates of AGB and so  
1503 should be avoided or minimised as far as possible. This is particularly important for large-scale site-to-site  
1504 comparison required for EO biomass product cal/val (e.g. for global FBRMS comparisons).

**Deleted:** Here, TLS data was collected using the highest LiDAR power (300 kHz) for RIEGL scanners VZ-400 and VZ-400i, trading off longer scan times for a fixed angular resolution to maximise coverage at the tops of tall trees.

- 1505 • **TLS processing** - broadly, TLS data acquisition and processing in tropical forests has gradually converged  
1506 towards something of a consensus, albeit this is still an active area of research and will vary depending on  
1507 the team, site and application. Specific issues to consider are the way in which trees are extracted from plot-  
1508 scale point clouds. Currently, the most accurate method for doing this is by manual cleaning of each tree  
1509 using a tool such as CloudCompare (CloudCompare Development Team, 2025). However, this is a time-  
1510 consuming and somewhat subjective process that is not fully replicable - different people will produce  
1511 slightly different results. Automated pipelines using machine learning/deep learning (ML/DL) offer a more  
1512 rapid and repeatable approach (e.g. Krisanski et al., 2021; Wilkes et al., 2023), however, their resulting tree  
1513 extraction accuracy is harder to assess given that the 'true' structure of trees is unknown. Manually-extracted  
1514 trees can be used to assess automated tree extraction accuracy, as well as forming the training data to enable  
1515 improvements in the underlying ML/DL approaches. Developing locally-trained / optimised ML/DL models  
1516 is likely to improve this approach further. Moving from individual tree point clouds to volume estimates it  
1517 is also important to use consistent QSM-fitting approaches. For example, there are systematic differences  
1518 between older and newer versions of TreeQSM, currently the most widely-used QSM fitting software  
1519 (Demol et al., 2024; Raumonen et al., 2013). Quantifying the uncertainty in tree-level estimates of volume  
1520 will depend on this processing chain, which will then determine the plot-level uncertainty when upscaling.
- 1521 • **UAV-LS acquisition and processing** - due to the wide range of platforms and LiDAR payloads being used  
1522 (as well as local UAV and safety regulations), there is currently little consensus in terms of both acquisition  
1523 and processing of UAV-LS data. There are a wide range of flight choices (particularly altitude), instrument  
1524 settings (scan angle), and survey systems (overlap, duration, etc.) that are a function of platform  
1525 performance, cost, etc. The impact of some of these choices is discussed in Brede et al. (2022b) where the  
1526 benefits of higher power, multiple returns and overlapping flights in detecting canopy structure are  
1527 highlighted. UAV-LS is not a like-for-like replacement for TLS, thus, the ability to compare these two

**Deleted:** r

**Deleted:** (h)

1534 different sources of LiDAR data will be facilitated by accurate geo-location (see above). This can be  
1535 achieved by using ground targets with surveyed locations that can be identified in the UAV-LS data (e.g.  
1536 reflective sheets/tarps, umbrellas, commercial UAV targets etc). This presupposes that there are sufficient  
1537 gaps in the canopy for targets to be seen, which is not always true. During data collection attention should  
1538 be paid to also either have access to GNSS observables from permanent base stations (e.g. CORS network)  
1539 or collect observables with a temporary base station (e.g. Emlid Reach RS+ or RS2). A base station should  
1540 be positioned less than 15 km away from the survey area. An important consideration for UAV-LS data  
1541 collection is whether visual line of sight ~~VLOS~~ needs to be maintained, i.e. visibility of the platform by the  
1542 pilot during the whole mission. If so, this can impact the choice of take-off, flight plan, etc. which in turn  
1543 may influence the choice of platform. Fixed-wing platforms have a much greater area coverage and flight  
1544 duration than VTOL platforms, but by necessity, must operate beyond VLOS (BVLOS). They also require  
1545 far more space to take off and land than VTOL platforms.

**Deleted:** ( )

- 1546 • **ALS acquisition and processing** - while ALS has been used operationally for forest applications for several  
1547 decades, its application for AGB estimates specifically is still less well-defined. In particular, this is true  
1548 when considering tree-scale rather than plot-level estimates. Practically, ALS surveys are almost always  
1549 outsourced (from the plot PIs, census and TLS, UAV teams) to commercial or agency (e.g. NASA, ESA,  
1550 NERC) providers. In the former case, there may be limited input from the end user over the platform,  
1551 instrument and acquisition parameters, or the way in which the data are processed to the resulting final  
1552 delivery. In ESA, NERC, NASA acquisitions, there tends to be more input from the users, but there may be  
1553 other restrictions in terms of when and where flights can be made. We recommend a pulse density of  $10 \text{ m}^{-2}$   
1554 or higher and a swath angle of +/-15 degrees or smaller. Most importantly, consistency over time of the  
1555 other acquisition parameters should be sought to enable meaningful temporal analysis of ALS point cloud.  
1556 In most cases, the 3D point cloud will be processed to generate a 2D canopy height model for further analysis.  
1557 This post-processing can have important effects on the results, we therefore, recommend users follow a  
1558 standardized procedure such as Fischer et al. (2024).

- 1559 • **Accurate (cm-scale) GNSS locations for 1ha FBRMS plot corners (or at the least the nominal origin 0, 0  
1560 coordinate for each plot):** this makes comparison and merging of any subsequent measurements much easier. It is  
1561 important to note that this is not a standard requirement of forest census measurements and requires specialist  
1562 surveying equipment e.g. GNSS RTK base station + rover configuration. It is also challenging under heavy forest  
1563 cover. Given that such setups are required (ideally) for TLS and UAV-LS, plot corner surveying is potentially best  
1564 carried out by these teams.
- 1565 • **Linking TLS trees to their census counterparts:** ideally, a permanent  $10 \times 10\text{m}$  subplot grid would be established  
1566 within each 1 ha forest plot. Census teams can then follow the same chain sampling pattern used in TLS data collection  
1567 (see Figure 2.1.4b & c) and identify the tree IDs found within each  $10 \times 10\text{ m}$  quadrants as they move through the

1570 plot. However, placing a 10 x 10 m sub-grid is not always straightforward (or even desirable) as it may require rebar  
1571 posts, which can be expensive and are likely to be removed or damaged by e.g. elephants in West African plots  
1572 particularly. An alternative approach is to label some trees with temporary numbered QR-type markers that can be  
1573 read automatically from the lidar point cloud data. The markers can be printed on A4 waterproof paper, attached to  
1574 trees with known census ID, and then identified in the TLS data using a tool such as qrDAR (Wilkes et al., 2017). If  
1575 the 20 or so largest trees are labelled in this way, distributed across a 1 ha plot, this makes subsequent tree matching  
1576 between census and TLS data much easier as there are known ‘anchor trees’ for the survey team to work from.

1577 **5. Data Access**

1578 This paper presents 30 datasets, comprising LiDAR and tree census data for all three ForestScan FBRMS. All datasets are  
1579 archived and publicly accessible through established data repositories. LiDAR datasets, including TLS, UAV-LS and ALS are  
1580 freely available from the CEDA Archive (<https://archive.ceda.ac.uk>) under the ForestScan data collection  
1581 (<https://dx.doi.org/10.5285/88a8620229014e0ebacf0606b302112d>; Chavana-Bryant et al., 2025b). This collection serves as  
1582 an umbrella repository linking all individual LiDAR datasets by site and acquisition type. All tree census datasets are provided  
1583 as curated data packages made available by the ForestPlots consortium and the French Agricultural Research Centre for  
1584 International Development (CIRAD) open-access portal.

1585  
1586 Tree census data packages for all three FBRMS are made available via two archival platforms: the CIRAD DataVerse portal  
1587 for French Guiana (<https://dataVERSE.cirad.fr/dataset.xhtml?persistentId=doi:10.18167/DVN1/94XHID>; Derroire et al., 2025),  
1588 while Gabon and Malaysian Borneo data are available through ForestPlots.net ([https://doi.org/10.5521/forestplots.net/2025\\_2](https://doi.org/10.5521/forestplots.net/2025_2);  
1589 Chavana-Bryant et al., 2025a). An additional census dataset for a non-ForestScan plot at FBRMS-01 is included in Table 10  
1590 and made available via the CEDA archive.

1591  
1592 Both tree census archival platforms operate under a fair use policy, governed by the Creative Commons Attribution-  
1593 NonCommercial-ShareAlike 4.0 International Licence (CC BY-NC-SA 4.0) (see <https://forestplots.net/en/join-forestplots/working-with-data> and <https://dataVERSE.org/best-practices/dataVERSE-community-norms>). These policies reflect a  
1594 strong commitment to equitable and inclusive data collection, funding, and sharing practices, as outlined in the ForestPlots  
1595 code of conduct (<https://forestplots.net/en/join-forestplots/code-of-conduct>). Tropical forest plot census data provide unique  
1596 insights into forest structure and dynamics but are challenging and often hazardous to collect, requiring sustained investment  
1597 and logistical support in remote regions with limited infrastructure. A persistent challenge to equitable research is that those  
1598 who collect these data are often least able to exploit the resulting large-scale datasets. This issue is particularly acute in the  
1599 context of commercial data exploitation, including by artificial intelligence and large-scale data mining enterprises. To address

1601 this, the ForestPlots community has developed data-sharing agreements that promote fairness and inclusivity, as detailed in de  
1602 Lima et al. (2022).

1603  
1604 Access and citation details for all ForestScan datasets are organised by site in Tables 10, 11, and 12 for FBRMS-01: Paracou,  
1605 French Guiana, FBRMS-02: Lopé National Park, Gabon, and FBRMS-03: Sepilok-Kabili, Malaysian Borneo, respectively.  
1606 Each table provides the specific data type, acquisition date, license type and citation format including DOI and URL for each  
1607 individual ForestScan dataset.

1608  
1609 **Table 10:** Dataset type, acquisition date, license type, and citation format including DOI and URL details for LiDAR (TLS,  
1610 UAV-LS and ALS) and tree census datasets available for FBRMS-01: Paracou, French Guiana. When using any of the  
1611 ForestScan datasets, this paper must also be cited.

ForestScan French Guiana Datasets / Acquisition date / Data license type	Data type	Citable as (DOI and URL included)
ForestScan Collection	Collection (multi-type composite of all ForestScan CEDA datasets)	Chavana-Bryant, C.; Wilkes, P.; Yang, W.; Burt, A.; Vines, P.; Bennett, A.C.; Pickavance, G.C.; Cooper, D.L.M.; Lewis, S.L.; Phillips, O.L.; Brede, B.; Lau, A.; Herold, M.; McNicol, I.M.; Mitchard, E.T.A.; Coombes, D.; Jackson, T.D.; Makaga, L.; Milamizokou Napo, H.O.; Ngomanda, A.; Ntie, S.; Medjibe, V.; Dimbonda, P.; Soenens, L.; Daelemans, V.; Proux, L.; Nilus, R.; Labrière, N.; Jeffery, K.; Burslem, D.F.R.P.; Clewley, D.; Moffat, D.; Qie, L.; Bartholomeus, H.; Vincent, G.; Barbier, N.; Derroire, G.; Abernethy, K.; Scipal, K.; Disney, M. (2025): ForestScan Collection, NERC EDS Centre for Environmental Data Analysis, 20 January 2025. DOI:10.5285/88a8620229014e0ebacf0606b302112d. <a href="https://catalogue.ceda.ac.uk/uuid/88a8620229014e0ebacf0606b302112d">https://catalogue.ceda.ac.uk/uuid/88a8620229014e0ebacf0606b302112d</a>
ForestScan Project: Terrestrial Laser Scanning (TLS) of FBRMS-01: Paracou, French Guiana 1ha plot FG5c1.  Acquisition date: Sep., Oct 2022  License type: CC BY 4.0 <a href="http://creativecommons.org/licenses/by/4.0/">http://creativecommons.org/licenses/by/4.0/</a>	TLS	Chavana-Bryant, C.; Wilkes, P.; Yang, W.; Burt, A.; Vines, P.; Bennett, A.C.; Pickavance, G.C.; Cooper, D.L.M.; Lewis, S.L.; Phillips, O.L.; Brede, B.; Lau, A.; Herold, M.; McNicol, I.M.; Mitchard, E.T.A.; Coombes, D.; Jackson, T.D.; Makaga, L.; Milamizokou Napo, H.O.; Ngomanda, A.; Ntie, S.; Medjibe, V.; Dimbonda, P.; Soenens, L.; Daelemans, V.; Proux, L.; Nilus, R.; Labrière, N.; Jeffery, K.; Burslem, D.F.R.P.; Clewley, D.; Moffat, D.; Qie, L.; Bartholomeus, H.; Vincent, G.; Barbier, N.; Derroire, G.; Abernethy, K.; Scipal, K.; Disney, M. (2025): ForestScan Project : Terrestrial Laser Scanning (TLS) of FBRMS-01: Paracou, French Guiana 1ha

**Deleted:** All LiDAR ForestScan datasets and one tree census dataset are freely available from the CEDA archive (<https://archive.ceda.ac.uk>) via the listed DOIs in Table 8a (Chavana-Bryant et al., 2025b). As previously mentioned in section 2.2.1, tree census data for FBRMS plots in Paracou, French Guiana is available as a data package via <https://dataVERSE.cirad.fr/dataset.xhtml?persistentId=doi:10.18167/DVN194XHID> (Derroire et al., 2025). Tree census data for FBRMS plots in Gabon and Malaysia are available as a data package via [https://doi.org/10.5521/forestplots.net/2025\\_2](https://doi.org/10.5521/forestplots.net/2025_2) (Chavana-Bryant et al., 2025a). Access, licensing and citation details for ForestScan tree inventory/census datasets: FBRMS-01 (French Guiana), FBRMS-02 (Gabon) and FBRMS-03 (Malaysian Borneo) are provided in Table 8b.¶ 1

**Deleted:** 8a

**Deleted:** Access

**Deleted:** ing

**Deleted:** 17

**Deleted:** one tree inventory/

**Deleted:** ForestScan

**Deleted:** in the CEDA archive

**Deleted:** Ois

**Formatted Table**

**Deleted:** ForestScan Collection

**Formatted:** Left

**Deleted:** [10.5285/656ac8ee1d42443f9addcbcc28c1b137](https://doi.org/10.5285/656ac8ee1d42443f9addcbcc28c1b137)

**Formatted Table**

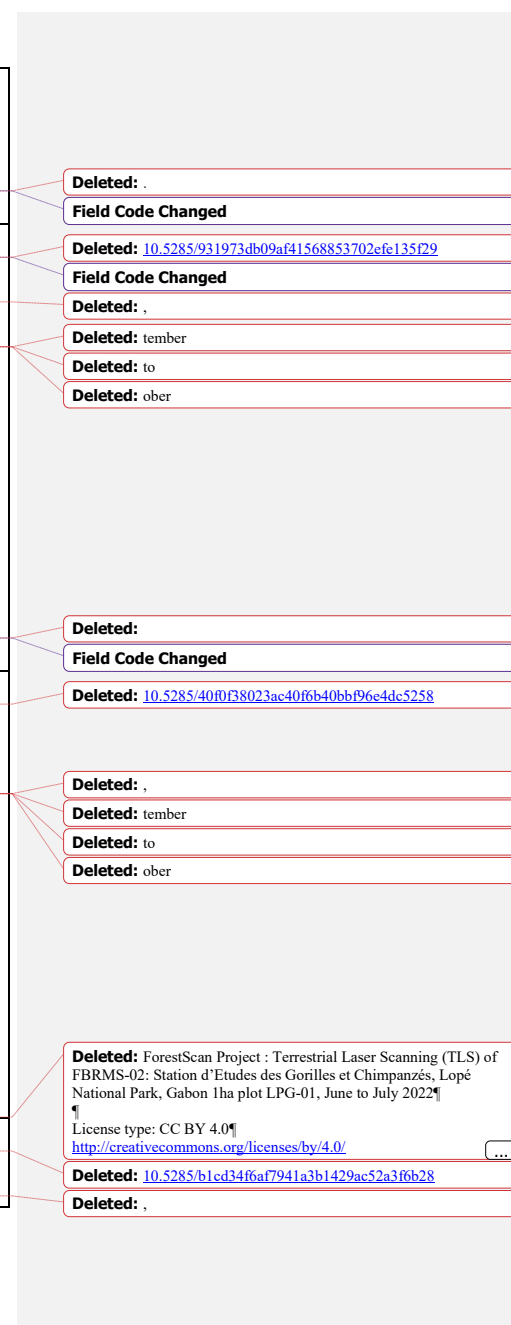
**Deleted:** ,

**Deleted:** tember

**Deleted:** to

**Deleted:** ober

		plot FG5c1, September to October 2022. NERC EDS Centre for Environmental Data Analysis, 28 March 2025. DOI:10.5285/656ac8ee1d42443f9addcbce28c1b137. <a href="https://dx.doi.org/10.5285/656ac8ee1d42443f9addcbce28c1b137">https://dx.doi.org/10.5285/656ac8ee1d42443f9addcbce28c1b137</a>
ForestScan Project: Terrestrial Laser Scanning (TLS) of FBRMS-01: Paracou, French Guiana 1ha plot FG6c2  <u>Acquisition date:</u> Sep, Oct 2022  License type: CC BY 4.0 <a href="http://creativecommons.org/licenses/by/4.0/">http://creativecommons.org/licenses/by/4.0/</a>	<u>TLS</u>	Chavana-Bryant, C.; Wilkes, P.; Yang, W.; Burt, A.; Vines, P.; Bennett, A.C.; Pickavance, G.C.; Cooper, D.L.M.; Lewis, S.L.; Phillips, O.L.; Brede, B.; Lau, A.; Herold, M.; McNicol, I.M.; Mitchard, E.T.A.; Coombes, D.; Jackson, T.D.; Makaga, L.; Milamizokou Napo, H.O.; Ngomanda, A.; Ntie, S.; Medjibe, V.; Dimbonda, P.; Soenens, L.; Daelemans, V.; Proux, L.; Nilus, R.; Labrière, N.; Jeffery, K.; Burslem, D.F.R.P.; Clewley, D.; Moffat, D.; Qie, L.; Bartholomeus, H.; Vincent, G.; Barbier, N.; Derroire, G.; Abernethy, K.; Scipal, K.; Disney, M. (2025): ForestScan Project : Terrestrial Laser Scanning (TLS) of FBRMS-01: Paracou, French Guiana 1ha plot FG6c2, September to October 2022. NERC EDS Centre for Environmental Data Analysis, 28 March 2025. DOI:10.5285/931973db09af41568853702efe135f29. <a href="https://dx.doi.org/10.5285/931973db09af41568853702efe135f29">https://dx.doi.org/10.5285/931973db09af41568853702efe135f29</a>
ForestScan Project: Terrestrial Laser Scanning (TLS) of FBRMS-01: Paracou, French Guiana 1ha plot FG8c4  <u>Acquisition date:</u> Sep, Oct 2022  License type: CC BY 4.0 <a href="http://creativecommons.org/licenses/by/4.0/">http://creativecommons.org/licenses/by/4.0/</a>	<u>TLS</u>	Chavana-Bryant, C.; Wilkes, P.; Yang, W.; Burt, A.; Vines, P.; Bennett, A.C.; Pickavance, G.C.; Cooper, D.L.M.; Lewis, S.L.; Phillips, O.L.; Brede, B.; Lau, A.; Herold, M.; McNicol, I.M.; Mitchard, E.T.A.; Coombes, D.; Jackson, T.D.; Makaga, L.; Milamizokou Napo, H.O.; Ngomanda, A.; Ntie, S.; Medjibe, V.; Dimbonda, P.; Soenens, L.; Daelemans, V.; Proux, L.; Nilus, R.; Labrière, N.; Jeffery, K.; Burslem, D.F.R.P.; Clewley, D.; Moffat, D.; Qie, L.; Bartholomeus, H.; Vincent, G.; Barbier, N.; Derroire, G.; Abernethy, K.; Scipal, K.; Disney, M. (2025): ForestScan Project : Terrestrial Laser Scanning (TLS) of FBRMS-01: Paracou, French Guiana 1ha plot FG8c4, September to October 2022. NERC EDS Centre for Environmental Data Analysis, 28 March 2025. DOI:10.5285/40f0f38023ac40f6b40bbf96e4dc5258. <a href="https://dx.doi.org/10.5285/40f0f38023ac40f6b40bbf96e4dc5258">https://dx.doi.org/10.5285/40f0f38023ac40f6b40bbf96e4dc5258</a>
ForestScan: Terrestrial Laser Scanning (TLS) of FBRMS-01: Paracou, French Guiana 1ha plot IRD-CNES (Tropiscat)	<u>TLS</u>	Vincent, G.; Villard, L. (2025): ForestScan: Terrestrial Laser Scanning (TLS) of FBRMS-01: Paracou, French Guiana 1ha plot IRD-CNES,



<p><u>Acquisition date:</u> Oct 2021</p> <p>License type: CC BY 4.0  <a href="http://creativecommons.org/licenses/by/4.0/">http://creativecommons.org/licenses/by/4.0/</a></p>		<p>October 2021. NERC EDS Centre for Environmental Data Analysis, 28 March 2025.</p> <p>DOI:10.5285/b1cd34f6af7941a3b1429ac52a3f6b28.<a href="https://dx.doi.org/10.5285/b1cd34f6af7941a3b1429ac52a3f6b28">h</a>  <a href="https://dx.doi.org/10.5285/b1cd34f6af7941a3b1429ac52a3f6b28">https://dx.doi.org/10.5285/b1cd34f6af7941a3b1429ac52a3f6b28</a></p>
<p>ForestScan Project: Unpiloted Aerial Vehicle LiDAR Scanning (UAV-LS) and Terrestrial Laser Scanning (TLS) data of FBRMS-01: Paracou, French Guiana plot 6.</p> <p><u>Acquisition date:</u> Oct – Nov 2019</p> <p>License type: CC BY 4.0  <a href="http://creativecommons.org/licenses/by/4.0/">http://creativecommons.org/licenses/by/4.0/</a></p>	<u>UAV-LS + TLS</u>	<p>Brede, B.; Barbier, N.; Bartholomeus, H.; Derroire, G.; Lau, A.; Lusk, D.; Herold, M. (2025): ForestScan Project: Unpiloted Aerial Vehicle LiDAR Scanning (UAV-LS) and Terrestrial Laser Scanning (TLS) data of FBRMS-01: Paracou, French Guiana plot 6, 10th October to 15th November 2019. NERC EDS Centre for Environmental Data Analysis, 28 March 2025.</p> <p>DOI:10.5285/325a4dde60d142049339e0c84816aac1  <a href="https://dx.doi.org/10.5285/325a4dde60d142049339e0c84816aac1">https://dx.doi.org/10.5285/325a4dde60d142049339e0c84816aac1</a></p>
<p>ForestScan Project: Multiple Unpiloted Aerial Vehicle LiDAR Scanning (UAV-LS) data acquisitions of FBRMS-01: Paracou, French Guiana, plots 4, 5, 6, 8, IRD-CNES (Tropiscat) and Flux-Tower area.</p> <p><u>Acquisition date:</u> Oct 2019</p> <p>License type: CC BY 4.0  <a href="http://creativecommons.org/licenses/by/4.0/">http://creativecommons.org/licenses/by/4.0/</a></p>	<u>UAV-LS</u>	<p>Barbier, N.; Vincent, G. (2025): ForestScan Project: Multiple Unpiloted Aerial Vehicle LiDAR Scanning (UAV-LS) data acquisitions of FBRMS-01: Paracou, French Guiana, plots 4, 5, 6, 8, IRD-CNES and Flux-Tower area, October 2019. NERC EDS Centre for Environmental Data Analysis, 28 March 2025.</p> <p>DOI:10.5285/005f2e0aebc24ed98a9772a0ba3798e2.  <a href="https://dx.doi.org/10.5285/005f2e0aebc24ed98a9772a0ba3798e2">https://dx.doi.org/10.5285/005f2e0aebc24ed98a9772a0ba3798e2</a></p>
<p>ForestScan: Aerial Laser Scanning (ALS) of FBRMS-01: Paracou, French Guiana</p> <p><u>Acquisition date:</u> Nov 2022</p> <p>License type: CC BY 4.0  <a href="http://creativecommons.org/licenses/by/4.0/">http://creativecommons.org/licenses/by/4.0/</a></p>	<u>ALS</u>	<p>Vincent, G. (2025): ForestScan: Aerial Laser Scanning (ALS) of FBRMS-01: Paracou, French Guiana, November 2022. NERC EDS Centre for Environmental Data Analysis, 28 March 2025.</p> <p>DOI:10.5285/7bef89a9dc404683a46642625a024a4b.  <a href="https://dx.doi.org/10.5285/7bef89a9dc404683a46642625a024a4b">https://dx.doi.org/10.5285/7bef89a9dc404683a46642625a024a4b</a></p>
<p>Aerial LiDAR (<u>ALS</u>) French Guiana Paracou.</p> <p><u>Acquisition date:</u> Nov 2019</p> <p>License type: CC BY 4.0  <a href="http://creativecommons.org/licenses/by/4.0/">http://creativecommons.org/licenses/by/4.0/</a></p>	<u>ALS</u>	<p>Jackson, T.D.; Vincent, G.; Coomes, D.A. (2023): Aerial LiDAR data from French Guiana, Paracou, November 2019. NERC EDS Centre for Environmental Data Analysis, 20 December 2023.</p> <p>DOI:10.5285/1d554ff41c104491ac3661c6f6f52aab.  <a href="https://dx.doi.org/10.5285/1d554ff41c104491ac3661c6f6f52aab">https://dx.doi.org/10.5285/1d554ff41c104491ac3661c6f6f52aab</a></p>
<p>Aerial LiDAR (<u>ALS</u>) French Guiana Nouragues</p> <p><u>Acquisition date:</u> Nov 2019</p>	<u>ALS</u> (additional non-ForestScan plot)	<p>Jackson, T.D.; Vincent, G.; Coomes, D.A. (2023): Aerial LiDAR data from French Guiana, Nouragues, November 2019. NERC EDS Centre for Environmental Data Analysis, 20 December 2023.</p> <p>DOI:10.5285/7bdc5bfc06264802be34f918597150e8.</p>

**Deleted:** ober

**Deleted:**

**Field Code Changed**

**Deleted:** <10.5285/325a4dde60d142049339e0c84816aac1>

**Deleted:** ,

**Deleted:** 10th

**Deleted:** ober to 15th November

**Deleted:** .

**Deleted:**

**Deleted:** <10.5285/005f2e0aebc24ed98a9772a0ba3798e2>

**Deleted:** ,

**Deleted:** ober

**Deleted:** ForestScan project: Unpiloted Aerial Vehicle LiDAR Scanning (UAV-LS) data of FBRMS-02: Station d'Etudes des Gorilles et Chimpanzés, Lopé National Park, Gabon, June 2022!  
<1>  
 License type: CC BY 4.0!  
<http://creativecommons.org/licenses/by/4.0/>

**Deleted:** <10.5285/7bef89a9dc404683a46642625a024a4b>

**Deleted:** ,

**Deleted:** ember

**Deleted:** <10.5285/1d554ff41c104491ac3661c6f6f52aab>

**Deleted:** ,

**Deleted:** ember

**Deleted:**

**Deleted:** <10.5285/7bdc5bfc06264802be34f918597150e8>

**Deleted:** ,

**Deleted:** ember

**Deleted:**

License type: CC BY 4.0 <a href="http://creativecommons.org/licenses/by/4.0/">http://creativecommons.org/licenses/by/4.0/</a>		<a href="https://dx.doi.org/10.5285/7bdc5bfc06264802be34f918597150e8">https://dx.doi.org/10.5285/7bdc5bfc06264802be34f918597150e8</a>
ForestScan: Plot descriptions for FBRMS-01: Paracou, French Guiana, 1ha plots FG5c1, FG6c2 and FG8c4  License: CC BY-NC-SA 4.0 <a href="http://creativecommons.org/licenses/by-nc-sa/4.0/">http://creativecommons.org/licenses/by-nc-sa/4.0/</a>	<a href="#">Tree census plot descriptions</a>	Derroire, G., Héault, B., Rossi, V., Blanc, L., Gourlet-Fleury, S., Schmitt, L., 2025, "ForestScan", 10.18167/DVN1/94XHID, CIRAD Dataverse, V1 <a href="https://dataverse.cirad.fr/dataset.xhtml?persistentId=doi:10.18167/DVN1/94XHID">https://dataverse.cirad.fr/dataset.xhtml?persistentId=doi:10.18167/DVN1/94XHID</a>
ForestScan: Tree census data for FBRMS-01: Paracou, French Guiana, 1ha plots FG5c1, FG6c2 and FG8c4  Acquisition date: FG5c1: Aug 2023 FG6c2: May - Jun 2023 FG8c4: Sep 2023  License: CC BY-NC-SA 4.0 <a href="http://creativecommons.org/licenses/by-nc-sa/4.0/">http://creativecommons.org/licenses/by-nc-sa/4.0/</a>	<a href="#">Tree census</a>	Derroire, G., Héault, B., Rossi, V., Blanc, L., Gourlet-Fleury, S., Schmitt, L., 2025, "ForestScan", 10.18167/DVN1/94XHID, CIRAD Dataverse, V1 <a href="https://dataverse.cirad.fr/dataset.xhtml?persistentId=doi:10.18167/DVN1/94XHID">https://dataverse.cirad.fr/dataset.xhtml?persistentId=doi:10.18167/DVN1/94XHID</a>
ForestScan: Tree census data (diameter and species name) of FBRMS-01: Paracou, French Guiana 1ha plot IRD-CNES (Tropiscat)  Acquisition date: Oct 2021  License type: CC BY 4.0 <a href="http://creativecommons.org/licenses/by/4.0/">http://creativecommons.org/licenses/by/4.0/</a>	<a href="#">Tree census (additional non-ForestScan plot)</a>	Vincent, G.; Martin, O.; Engel, F. (2025): ForestScan: Tree census data (diameter and species name) of FBRMS-01: Paracou, French Guiana 1ha plot IRD-CNES, October 2021. NERC EDS Centre for Environmental Data Analysis, 28 March 2025. DOI:10.5285/5e78ff91e9cd4143bfa3b7358efd2607. <a href="https://dx.doi.org/10.5285/5e78ff91e9cd4143bfa3b7358efd2607">https://dx.doi.org/10.5285/5e78ff91e9cd4143bfa3b7358efd2607</a>

**Deleted:**

**Deleted:** Airborne LiDAR and RGB imagery from Sepilok Reserve and Danum Valley in Malaysia in 2020  
¶  
License type: OGL UK 3.0¶<https://www.nationalarchives.gov.uk/doc/open-government-licence/version/3/>

**Field Code Changed**

**Formatted:** No Spacing

**Field Code Changed**

**Formatted:** Line spacing: single

**Field Code Changed**

**Formatted:** Line spacing: single

**Field Code Changed**

**Deleted:** [10.5285/5e78ff91e9cd4143bfa3b7358efd2607](https://doi.org/10.5285/5e78ff91e9cd4143bfa3b7358efd2607)

**Deleted:** ,

**Deleted:** ober

**Deleted:**

**Field Code Changed**

1689  
1690 **Table 10:** Dataset type, acquisition date, license type, and citation format including DOI and URL details for LiDAR (TLS, UAV-LS and ALS) and tree census datasets available for FBRMS-02: Lopé, Gabon. When using any of the ForestScan  
1691 datasets, this paper must also be cited.  
1692

ForestScan Gabon Datasets / Acquisition date / Data license type	Data type	Citable as (DOI and URL included)
ForestScan Project : Terrestrial Laser Scanning (TLS) of FBRMS-02: Station d'Etudes des Gorilles et Chimpanzés, Lopé National Park, Gabon 1ha plot LPG-01  Acquisition date: Jun - Jul 2022	<a href="#">TLS</a>	Chavana-Bryant, C.; Wilkes, P.; Yang, W.; Burt, A.; Vines, P.; Bennett, A.C.; Pickavance, G.C.; Cooper, D.L.M.; Lewis, S.L.; Phillips, O.L.; Brede, B.; Lau, A.; Herold, M.; McNicol, I.M.; Mitchard, E.T.A.; Coombes, D.; Jackson, T.D.; Makaga, L.; Milamizokou Napo, H.O.; Ngomanda, A.; Ntie, S.;

**Formatted Table**

**Formatted:** Font: Bold

<p>License type: CC BY 4.0  <a href="http://creativecommons.org/licenses/by/4.0/">http://creativecommons.org/licenses/by/4.0/</a></p>		<p><u>Medjibe, V.; Dimbonda, P.; Soenens, L.; Daelemans, V.; Proux, L.; Nilus, R.; Labrière, N.; Jeffery, K.; Burslem, D.F.R.P.; Clewley, D.; Moffat, D.; Qie, L.; Bartholomeus, H.; Vincent, G.; Barbier, N.; Derroire, G.; Abernethy, K.; Scipal, K.; Disney, M. (2025): ForestScan Project : Terrestrial Laser Scanning (TLS) of FBRMS-02: Station d'Etudes des Gorilles et Chimpanzés, Lopé National Park, Gabon 1ha plot LPG-01, June to July 2022. NERC EDS Centre for Environmental Data Analysis, 28 March 2025.</u>  <u>DOI:10.5285/8ea2c697ee53430a84825384bfdf06a.</u>  <u><a href="https://dx.doi.org/10.5285/8ea2c697ee53430a84825384bfdf06a">https://dx.doi.org/10.5285/8ea2c697ee53430a84825384bfdf06a</a></u></p>
<p><u>ForestScan Project : Terrestrial Laser Scanning (TLS) of FBRMS-02: Station d'Etudes des Gorilles et Chimpanzés, Lopé National Park, Gabon 1ha plot OKO-01</u></p> <p><u>Acquisition date: Jun - Jul 2022</u></p> <p>License type: CC BY 4.0  <a href="http://creativecommons.org/licenses/by/4.0/">http://creativecommons.org/licenses/by/4.0/</a></p>	<p><u>TLS</u></p>	<p><u>Chavana-Bryant, C.; Wilkes, P.; Yang, W.; Burt, A.; Vines, P.; Bennett, A.C.; Pickavance, G.C.; Cooper, D.L.M.; Lewis, S.L.; Phillips, O.L.; Brede, B.; Lau, A.; Herold, M.; McNicol, I.M.; Mitchard, E.T.A.; Coombes, D.; Jackson, T.D.; Makaga, L.; Milamizokou Napo, H.O.; Ngomanda, A.; Ntie, S.; Medjibe, V.; Dimbonda, P.; Soenens, L.; Daelemans, V.; Proux, L.; Nilus, R.; Labrière, N.; Jeffery, K.; Burslem, D.F.R.P.; Clewley, D.; Moffat, D.; Qie, L.; Bartholomeus, H.; Vincent, G.; Barbier, N.; Derroire, G.; Abernethy, K.; Scipal, K.; Disney, M. (2025): ForestScan Project : Terrestrial Laser Scanning (TLS) of FBRMS-02: Station d'Etudes des Gorilles et Chimpanzés, Lopé National Park, Gabon 1ha plot OKO-01, June to July 2022. NERC EDS Centre for Environmental Data Analysis, 28 March 2025.</u>  <u>DOI:10.5285/45ae3437f82f4e4fb759a5c26a194ba.</u>  <u><a href="https://dx.doi.org/10.5285/45ae3437f82f4e4fb759a5c26a194ba">https://dx.doi.org/10.5285/45ae3437f82f4e4fb759a5c26a194ba</a></u></p>
<p><u>ForestScan Project : Terrestrial Laser Scanning (TLS) of FBRMS-02: Station d'Etudes des Gorilles et Chimpanzés, Lopé National Park, Gabon 1ha plot OKO-02</u></p> <p><u>Acquisition date: Jun - Jul 2022</u></p> <p>License type: CC BY 4.0  <a href="http://creativecommons.org/licenses/by/4.0/">http://creativecommons.org/licenses/by/4.0/</a></p>	<p><u>TLS</u></p>	<p><u>Chavana-Bryant, C.; Wilkes, P.; Yang, W.; Burt, A.; Vines, P.; Bennett, A.C.; Pickavance, G.C.; Cooper, D.L.M.; Lewis, S.L.; Phillips, O.L.; Brede, B.; Lau, A.; Herold, M.; McNicol, I.M.; Mitchard, E.T.A.; Coombes, D.; Jackson, T.D.; Makaga, L.; Milamizokou Napo, H.O.; Ngomanda, A.; Ntie, S.; Medjibe, V.; Dimbonda, P.; Soenens, L.; Daelemans, V.; Proux, L.; Nilus, R.; Labrière, N.; Jeffery, K.; Burslem, D.F.R.P.; Clewley, D.; Moffat, D.; Qie, L.; Bartholomeus, H.; Vincent, G.; Barbier, N.; Derroire, G.; Abernethy, K.; Scipal, K.; Disney, M. (2025): ForestScan Project : Terrestrial Laser Scanning (TLS) of FBRMS-02: Station d'Etudes des Gorilles et Chimpanzés, Lopé National Park, Gabon 1ha plot OKO-02, June to July 2022. NERC EDS Centre for Environmental Data Analysis, 28 March 2025.</u></p>

		<p>DOI:10.5285/ff4b43475c9641cca1dad2c8be8dadaf. <a href="https://dx.doi.org/10.5285/ff4b43475c9641cca1dad2c8be8dadaf">https://dx.doi.org/10.5285/ff4b43475c9641cca1dad2c8be8dadaf</a></p>
<p><a href="#">ForestScan Project : Terrestrial Laser Scanning (TLS) of FBRMS-02: Station d'Etudes des Gorilles et Chimpanzés, Lopé National Park, Gabon 1ha plot OKO-03</a></p> <p><a href="#">Acquisition date: Jun - Jul 2022</a></p> <p><a href="#">License type: CC BY 4.0</a> <a href="http://creativecommons.org/licenses/by/4.0/">http://creativecommons.org/licenses/by/4.0/</a></p>	<p><a href="#">TLS</a></p>	<p>Chavana-Bryant, C.; Wilkes, P.; Yang, W.; Burt, A.; Vines, P.; Bennett, A.C.; Pickavance, G.C.; Cooper, D.L.M.; Lewis, S.L.; Phillips, O.L.; Brede, B.; Lau, A.; Herold, M.; McNicol, I.M.; Mitchard, E.T.A.; Coombes, D.; Jackson, T.D.; Makaga, L.; Milamizokou Napo, H.O.; Ngomanda, A.; Ntie, S.; Medjibe, V.; Dimbonda, P.; Soenens, L.; Daelemans, V.; Proux, L.; Nilus, R.; Labrière, N.; Jeffery, K.; Burslem, D.F.R.P.; Clewley, D.; Moffat, D.; Qie, L.; Bartholomeus, H.; Vincent, G.; Barbier, N.; Derroire, G.; Abernethy, K.; Scipal, K.; Disney, M. (2025): ForestScan Project : Terrestrial Laser Scanning (TLS) of FBRMS-02: Station d'Etudes des Gorilles et Chimpanzés, Lopé National Park, Gabon 1ha plot OKO-03, June to July 2022. NERC EDS Centre for Environmental Data Analysis, 28 March 2025. DOI:10.5285/8ed3ddec76b8470285bdb2ea643f54bc. <a href="https://dx.doi.org/10.5285/8ed3ddec76b8470285bdb2ea643f54bc">https://dx.doi.org/10.5285/8ed3ddec76b8470285bdb2ea643f54bc</a></p>
<p><a href="#">ForestScan project: Unpiloted Aerial Vehicle LiDAR Scanning (UAV-LS) data of FBRMS-02: Station d'Etudes des Gorilles et Chimpanzés, Lopé National Park, Gabon</a></p> <p><a href="#">Acquisition date: Jun 2022</a></p> <p><a href="#">License type: CC BY 4.0</a> <a href="http://creativecommons.org/licenses/by/4.0/">http://creativecommons.org/licenses/by/4.0/</a></p>	<p><a href="#">UAV-LS</a></p>	<p>McNicol, I.M.; Mitchard, E.T.A. (2025): ForestScan project: Unpiloted Aerial Vehicle LiDAR Scanning (UAV-LS) data of FBRMS-02: Station d'Etudes des Gorilles et Chimpanzés, Lopé National Park, Gabon, June 2022. NERC EDS Centre for Environmental Data Analysis, 28 March 2025. DOI:10.5285/a79fc9ab0c443fc86d453cc064759b. <a href="https://dx.doi.org/10.5285/a79fc9ab0c443fc86d453cc064759b">https://dx.doi.org/10.5285/a79fc9ab0c443fc86d453cc064759b</a></p>
<p><a href="#">ForestScan: Tree census data for FBRMS-02: Lope, Gabon, 1ha plots LPG-01, OKO-01, OKO-02 and OKO-03</a></p> <p><a href="#">Acquisition date: LPG-01: Feb 2022</a> <a href="#">OKO-01: Mar 2022</a> <a href="#">OKO-02: Feb 2022</a> <a href="#">OKO-03: Feb 2022</a></p> <p><a href="#">License: CC BY-NC-SA 4.0</a> <a href="http://creativecommons.org/licenses/by-nc-sa/4.0/">http://creativecommons.org/licenses/by-nc-sa/4.0/</a></p>	<p><a href="#">Tree census</a></p>	<p>Chavana-Bryant, C., Wilkes, P., Yang, W., Burt, A., Vines, P., Bennett, A.C., Pickavance, G., Cooper, D.L.M., Lewis, S.L., Phillips, O.L., Brede, B., Lau, A., Herold, M., McNicol, I.M., Mitchard, E.T.A., Barbier, N., Vincent, G., Coomes, D.A., Jackson, T., Makaga, L., Milamizokou Napo, H.O., Ngomanda, A., Ntie, S., Medjibe, V., Dimbonda, P., Soenens, L., Daelemans, V., Bartholomeus, H., Majalap, N., Nilus, R., Labrière, N., Burslem, D.F.R.P., Qie, L., Derroire, G., Proux, L., Abernethy, K., Jeffery, K., Clewley, D., Moffat, D., Scipal, K. and Disney, M. ForestScan: a unique multiscale dataset of tropical forest structure across 3 continents including terrestrial, UAV and airborne LiDAR and in-situ forest census data. ESSD. 2025</p>

		<a href="https://doi.org/10.5521/forestplots.net/2025_2">DOI: 10.5521/forestplots.net/2025_2</a> <a href="https://doi.org/10.5521/forestplots.net/2025_2">https://doi.org/10.5521/forestplots.net/2025_2</a>
--	--	---

1704  
1705 **Table 11:** Dataset type, acquisition date, license type, and citation format including DOI and URL details for LiDAR (TLS,  
1706 UAV-LS and ALS) and tree census datasets available for FBRMS-03: Kabili-Sepilok, Malaysian Borneo. When using any of  
1707 the ForestScan datasets, this paper must also be cited.

<a href="#"><u>ForestScan Malaysian Borneo Datasets / Acquisition date / Data license type</u></a>	<a href="#"><u>Data type</u></a>	<a href="#"><u>Citable as (DOI and URL included)</u></a>
<p><a href="#"><u>ForestScan Project : Terrestrial Laser Scanning (TLS) of FBRMS-03: Kabili-Sepilok, Malaysian Borneo 1ha plot SEP-11</u></a></p> <p><a href="#"><u>Acquisition date: Mar 2017</u></a></p> <p><a href="#"><u>License type: CC BY 4.0</u></a>  <a href="http://creativecommons.org/licenses/by/4.0/">http://creativecommons.org/licenses/by/4.0/</a></p>	<a href="#"><u>TLS</u></a>	<p><a href="#"><u>Chavana-Bryant, C.; Wilkes, P.; Yang, W.; Burt, A.; Vines, P.; Bennett, A.C.; Pickavance, G.C.; Cooper, D.L.M.; Lewis, S.L.; Phillips, O.L.; Brede, B.; Lau, A.; Herold, M.; McNicol, I.M.; Mitchard, E.T.A.; Coombes, D.; Jackson, T.D.; Makaga, L.; Milamizokou Napo, H.O.; Ngomanda, A.; Ntie, S.; Mediibe, V.; Dimbonda, P.; Soenens, L.; Daelemans, V.; Proux, L.; Nilus, R.; Labrière, N.; Jeffery, K.; Burslem, D.F.R.P.; Clewley, D.; Moffat, D.; Qie, L.; Bartholomeus, H.; Vincent, G.; Barbier, N.; Derroire, G.; Abernethy, K.; Scipal, K.; Disney, M. (2025): ForestScan Project : Terrestrial Laser Scanning (TLS) of FBRMS-03: Kabili-Sepilok, Malaysian Borneo 1ha plot SEP-11, March 2017. NERC EDS Centre for Environmental Data Analysis, 28 March 2025.</u></a></p> <p><a href="#"><u>DOI:10.5285/37b039605e9b4bb5a89371fd7f5b7ba1.</u></a>  <a href="https://dx.doi.org/10.5285/37b039605e9b4bb5a89371fd7f5b7ba1">https://dx.doi.org/10.5285/37b039605e9b4bb5a89371fd7f5b7ba1</a></p>
<p><a href="#"><u>ForestScan Project : Terrestrial Laser Scanning (TLS) of FBRMS-03: Kabili-Sepilok, Malaysian Borneo 1ha plot SEP-12</u></a></p> <p><a href="#"><u>Acquisition date: Mar 2017</u></a></p> <p><a href="#"><u>License type: CC BY 4.0</u></a>  <a href="http://creativecommons.org/licenses/by/4.0/">http://creativecommons.org/licenses/by/4.0/</a></p>	<a href="#"><u>TLS</u></a>	<p><a href="#"><u>Chavana-Bryant, C.; Wilkes, P.; Yang, W.; Burt, A.; Vines, P.; Bennett, A.C.; Pickavance, G.C.; Cooper, D.L.M.; Lewis, S.L.; Phillips, O.L.; Brede, B.; Lau, A.; Herold, M.; McNicol, I.M.; Mitchard, E.T.A.; Coombes, D.; Jackson, T.D.; Makaga, L.; Milamizokou Napo, H.O.; Ngomanda, A.; Ntie, S.; Mediibe, V.; Dimbonda, P.; Soenens, L.; Daelemans, V.; Proux, L.; Nilus, R.; Labrière, N.; Jeffery, K.; Burslem, D.F.R.P.; Clewley, D.; Moffat, D.; Qie, L.; Bartholomeus, H.; Vincent, G.; Barbier, N.; Derroire, G.; Abernethy, K.; Scipal, K.; Disney, M. (2025): ForestScan Project : Terrestrial Laser Scanning (TLS) of FBRMS-03: Kabili-Sepilok, Malaysian Borneo 1ha plot SEP-12, March 2017. NERC EDS Centre for Environmental Data Analysis, 28 March 2025.</u></a></p> <p><a href="#"><u>DOI:10.5285/bb81c82352524df99ddd411f6ca2ec81.</u></a></p>

1704  
1705  
1706  
1707 Formatted Table

		<a href="https://dx.doi.org/10.5285/bb81c82352524df99ddd411f6ca2ec81">https://dx.doi.org/10.5285/bb81c82352524df99ddd411f6ca2ec81</a>
<p><a href="#">ForestScan Project: Terrestrial Laser Scanning (TLS) of FBRMS-03: Kabili-Sepilok, Malaysian Borneo 1ha plot SEP-30</a></p> <p><a href="#">Acquisition date: Mar 2017</a></p> <p><a href="#">License type: CC BY 4.0</a>  <a href="http://creativecommons.org/licenses/by/4.0/">http://creativecommons.org/licenses/by/4.0/</a></p>	<a href="#">TLS</a>	<p>Chavana-Bryant, C.; Wilkes, P.; Yang, W.; Burt, A.; Vines, P.; Bennett, A.C.; Pickavance, G.C.; Cooper, D.L.M.; Lewis, S.L.; Phillips, O.L.; Brede, B.; Lau, A.; Herold, M.; McNicol, I.M.; Mitchard, E.T.A.; Coombes, D.; Jackson, T.D.; Makaga, L.; Milamizokou Napo, H.O.; Ngomanda, A.; Ntie, S.; Medjibe, V.; Dimbonda, P.; Soenens, L.; Daelemans, V.; Proux, L.; Nilus, R.; Labrière, N.; Jeffery, K.; Burslem, D.F.R.P.; Clewley, D.; Moffat, D.; Qie, L.; Bartholomeus, H.; Vincent, G.; Barbier, N.; Derroire, G.; Abernethy, K.; Scipal, K.; Disney, M. (2025): ForestScan Project : Terrestrial Laser Scanning (TLS) of FBRMS-03: Kabili-Sepilok, Malaysian Borneo 1ha plot SEP-30, March 2017. NERC EDS Centre for Environmental Data Analysis, 28 March 2025.</p> <p>DOI:10.5285/ff217c783e3f4c66a4891d2b5807ee6e.  <a href="https://dx.doi.org/10.5285/ff217c783e3f4c66a4891d2b5807ee6e">https://dx.doi.org/10.5285/ff217c783e3f4c66a4891d2b5807ee6e</a></p>
<p><a href="#">Airborne LiDAR and RGB imagery from Sepilok Reserve and Danum Valley in Malaysia</a></p> <p><a href="#">Acquisition date: Feb 2020</a></p> <p><a href="#">License type: OGL UK 3.0</a>  <a href="https://www.nationalarchives.gov.uk/doc/open-government-licence/version/3/">https://www.nationalarchives.gov.uk/doc/open-government-licence/version/3/</a></p>	<a href="#">ALS</a>	<p>Coomes, D.A.; Jackson, T.D. (2022): Airborne LiDAR and RGB imagery from Sepilok Reserve and Danum Valley in Malaysia in 2020. NERC EDS Centre for Environmental Data Analysis, 03 October 2022.</p> <p>DOI:10.5285/dd4d20c8626f4b9d99bc14358b1b50fe.  <a href="https://dx.doi.org/10.5285/dd4d20c8626f4b9d99bc14358b1b50fe">https://dx.doi.org/10.5285/dd4d20c8626f4b9d99bc14358b1b50fe</a></p>
<p><a href="#">ForestScan: Tree census data for FBRMS-03: Kabili-Sepilok, Malaysian Borneo, plots SEP-11, SEP-12 and SEP-30</a></p> <p><a href="#">Acquisition date: SEP-11: Jan 2020</a>  <a href="#">SEP-12: Mar 2020</a>  <a href="#">SEP-30: Jun 2021</a></p> <p><a href="#">License: CC BY-NC-SA 4.0</a>  <a href="http://creativecommons.org/licenses/by-nc-sa/4.0/">http://creativecommons.org/licenses/by-nc-sa/4.0/</a></p>	<a href="#">Tree census</a>	<p>Chavana-Bryant, C., Wilkes, P., Yang, W., Burt, A., Vines, P., Bennett, A.C., Pickavance, G., Cooper, D.L.M., Lewis, S.L., Phillips, O.L., Brede, B., Lau, A., Herold, M., McNicol, I.M., Mitchard, E.T.A., Barbier, N., Vincent, G., Coomes, D.A., Jackson, T., Makaga, L., Milamizokou Napo, H.O., Ngomanda, A., Ntie, S., Medjibe, V., Dimbonda, P., Soenens, L., Daelemans, V., Bartholomeus, H., Majalap, N., Nilus, R., Labrière, N., Burslem, D.F.R.P., Qie, L., Derroire, G., Proux, L., Abernethy, K., Jeffery, K., Clewley, D., Moffat, D., Scipal, K. and Disney, M. ForestScan: a unique multiscale dataset of tropical forest structure across 3 continents including terrestrial, UAV and airborne LiDAR and in-situ forest census data. ESSD, 2025</p> <p>DOI: 10.5521/forestplots.net/2025_2  <a href="https://doi.org/10.5521/forestplots.net/2025_2">https://doi.org/10.5521/forestplots.net/2025_2</a></p>

Field Code Changed

Formatted: Left

Formatted: Font: (Default) Times New Roman, Underline, Font color: Blue, Pattern: Clear

Formatted: No Spacing

Field Code Changed

1708  
1709

1711 **6. Author contributions**

1712 All authors provided input towards the writing of this manuscript.

1713 C.Ch.-B. wrote the manuscript with significant input from M.D.

1714 C.Ch.-B. developed the TLS data processing pipeline.

1715 C.Ch.-B. collected, cleaned, processed and curated TLS data.

1716 C.Ch.-B. developed the data repositories and ensured data integrity with support from M.D., the CEDA data management team  
1717 and the ForestPlots and DataVerse database management teams.

1718 P.W. developed the TLS data processing pipeline. assisted in the collection of TLS data in FBRMS-02: Lopé, Gabon and its  
1719 processing.

1720 W.Y. developed the TLS data processing pipeline. assisted in the collection of TLS data in FBRMS-01 Paracou, French Guiana  
1721 and its processing.

1722 A.B., and T.J. collected TLS data in FBRMS-03: Kabilis-Sepilok, Malaysian Borneo.

1723 H.O.M.N. and L.M. provided field logistics and assisted in the collection of TLS data in FBRMS-02: Lopé, Gabon

1724 L.S. and V. D. helped collect TLS in FBRMS-02: Lopé, Gabon.

1725 K.A., S.N. & A.N. provided logistics and research permit support for FBRMS-02: Lopé, Gabon.

1726 P.V. assisted in the processing of TLS data and developing the TLS2trees Processing Scripts.

1727 A.C.B. collected census data in FBRMS-01 Paracou, French Guiana and in FBRMS-02: Lopé, Gabon with assistance from  
1728 D.L.M.C.

1729 V.M., P.D, H.O.M.N. and K.J collected the field census data for LPG-01

1730 N.L., P.D., H.O.M.N. and K.J. collected the field census data for OKO-01, OKO-02 and OKO-03 in Lopé, Gabon.

1731 T.J., D.C. and G.V. planned and funded the ALS data collection in FBRMS-01, Paracou French Guiana.

1732 T.J. & D.C. planned and funded the ALS data collection in FBRMS-03, Kabilis-Sepilok, Malaysian Borneo.

1733 I.M.M. arranged, collected and processed the UAV-LS data collected over FBRMS-02: Lopé, Gabon.

1734 B.B., A.L. and H.B. collected, cleaned, processed and curated TLS and UAV-LS data collected at Paracou, French Guiana.

1735 N.B., G.V. collected, cleaned, processed and curated TLS and UAV-LS data collected at Paracou, French Guiana.

1736 **7. Competing interests**

1737 A.B. is an employee and/or shareowner of Sylvera Ltd. All other authors declare that they have no conflict of interest.

**Deleted:** Table 8b: Access, licensing and citation details for ForestScan tree inventory/census datasets: FBRMS-01 (French Guiana), FBRMS-02 (Gabon) and FBRMS-03 (Malaysian Borneo). When using any of the ForestScan datasets, this paper must also be cited.¶

These datasets are provided as curated data packages made available by the ForestPlots consortium and the French Agricultural Research Centre for International Development (CIRAD) open-access portal – DataVerse. Both archival platforms operate under a fair use policy, governed by the Creative Commons Attribution-NonCommercial-ShareAlike 4.0 International Licence (CC BY-NC-SA 4.0) (see <https://forestplots.net/en/join-forestplots/working-with-data> and <https://dataVERSE.org/best-practices/dataverse-community-norms>). These policies reflect a strong commitment to equitable and inclusive data collection, funding, and sharing practices, as outlined in the ForestPlots code of conduct (<https://forestplots.net/en/join-forestplots/code-of-conduct>).¶

Tropical forest plot census data provide unique insights into forest structure and dynamics but are challenging and often hazardous to collect, requiring sustained investment and logistical support in remote regions with limited infrastructure. A persistent challenge to equitable research is that those who collect these data are often least able to exploit the resulting large-scale datasets. This issue is particularly acute in the context of commercial data exploitation, including by artificial intelligence and large-scale data mining enterprises. To address this, the ForestPlots community has developed data-sharing agreements that promote fairness and inclusivity, as detailed in de Lima et al. (2022).¶

¶ ForestScan Datasets / ¶  
Data license type

These datasets are provided as curated data packages made available by the ForestPlots consortium and the French Agricultural Research Centre for International Development (CIRAD) open-access portal – DataVerse. Both archival platforms operate under a fair use policy, governed by the Creative Commons Attribution-NonCommercial-ShareAlike 4.0 International Licence (CC BY-NC-SA 4.0) (see <https://forestplots.net/en/join-forestplots/working-with-data> and <https://dataVERSE.org/best-practices/dataverse-community-norms>). These policies reflect a strong commitment to equitable and inclusive data collection, funding, and sharing practices, as outlined in the ForestPlots code of conduct (<https://forestplots.net/en/join-forestplots/code-of-conduct>).¶

Tropical forest plot census data provide unique insights into forest structure and dynamics but are challenging and often hazardous to collect, requiring sustained investment and logistical support in remote regions with limited infrastructure. A persistent challenge to equitable research is that those who collect these data are often least able to exploit the resulting large-scale datasets. This issue is particularly acute in the context of commercial data exploitation, including by artificial intelligence and large-scale data mining enterprises. To address this, the ForestPlots community has developed data-sharing agreements that promote fairness and inclusivity, as detailed in de Lima et al. (2022).¶

¶ ForestScan Datasets / ¶  
Data license type

1795 **8. Acknowledgements**

1796 We are indebted to the long-term work of many researchers in funding, establishing and maintaining the field plots that were  
1797 used in this study. It is not possible to carry out meaningful cal/val measurements of tropical forest biomass for earth  
1798 observation studies without the logistical support and expertise of the plot PIs and their teams. We thank Dr Noreen Majalap  
1799 for logistical and research permit support in FBRMS-03, Kabil-Sepilok, Malaysian Borneo. We also thank the Sabah  
1800 Biodiversity Council for their support with airborne laser scanning data collection in Kabil-Sepilok, access license number:  
1801 JKM/MBS.1000-2/2 JLD.9 (122). We thank Esther Conway and her team for their outstanding support in developing the  
1802 ForestScan CEDA dataset collection. We thank Dr Aurora Levesley and Gaëlle Jaouen for their generous support in developing  
1803 the ForestPlots and DataVerse tree census data packages. Specific data collection activities were funded by the European Space  
1804 Agency under ESA/ contract No. 4000126857/20/NL/AI. Work in French Guiana benefited from the Investissement d'Avenir  
1805 grants of the ANR, France (CEBA: ANR-10-LABX-0025). M.D., P.W., C.Ch.-B., W.Y. acknowledge capital funding for TLS  
1806 equipment from UCL Geography and the NERC National Centre for Earth Observation (NCEO). T.J. and D.C. acknowledge  
1807 the funding for ~~ALS~~ data collection over FBRMS-01 Paracou, French Guiana in 2019 and FBRMS-03: Kabil-Sepilok,  
1808 Malaysian Borneo during February 2020 as part of a NERC project grant (NE/S010750/1). I.M.M. was partly funded by a  
1809 European Research Council Starting Grant (757526) awarded to E.T.A.M. Work in Lopé was supported by core funding from  
1810 Total Gabon and the EU-ACP ECOFAC VI grant to the Gabon National Parks Agency for logistics, staff and site operations.  
1811

**Deleted:** airborne laser scanning (

**Deleted:** )

## 9. References

1815 R package Geomorph: Geometric Morphometric Analyses of 3D Data: <https://rdrr.io/cran/geomorph/man/read.ply.html>, last access: November 2025. Formatted: Space After: 6 pt

1816

1817 Agence Nationale des Parcs Nationaux (ANPN): Parcs Gabon, Recherche Scientifique: <https://scienceparcs gabon.weebly.com/>, last access: November 2024.

1818

1819 Askne, J. and Santoro, M.: Experiences in boreal forest stem volume estimation from multitemporal C-band InSAR, in: Recent Interferometry Applications in Topography and Astronomy, 169-194, 2012.

1820

1821 Avitabile, V., Herold, M., Henry, M., and Schmullius, C.: Mapping biomass with remote sensing: a comparison of methods for the case study of Uganda, Carbon balance and management, 6, 1-14, 10.1186/1750-0680-6-7, 2011.

1822

1823 Avitabile, V., Herold, M., Heuvelink, G. B., Lewis, S. L., Phillips, O. L., Asner, G. P., Armston, J., Ashton, P. S., Banin, L., and Bayol, N.: An integrated pan-tropical biomass map using multiple reference datasets, Global change biology, 22, 1406-1420, 10.1111/gcb.13139, 2016.

1824

1825

1826 Brede, B., Bartholomeus, H. M., Barbier, N., Pimont, F., Vincent, G., and Herold, M.: Peering through the thicket: Effects of UAV LiDAR scanner settings and flight planning on canopy volume discovery, International Journal of Applied Earth Observation and Geoinformation, 114, 103056, 10.1016/j.jag.2022.103056, 2022b.

1827

1828

1829 Brede, B., Terryn, L., Barbier, N., Bartholomeus, H. M., Bartolo, R., Calders, K., Derroire, G., Moorthy, S. M. K., Lau, A., and Levick, S. R.: Non-destructive estimation of individual tree biomass: Allometric models, terrestrial and UAV laser scanning, Remote Sensing of Environment, 280, 113180, 10.1016/j.rse.2022.113180, 2022a.

1830

1831

1832 Burt, A., Disney, M., and Calders, K.: Extracting individual trees from lidar point clouds using treeseg, Methods in Ecology and Evolution, 10, 438-445, 10.1111/2041-210x.13121, 2019.

1833

1834 Burt, A., Calders, K., Cuni-Sánchez, A., Gómez-Dans, J., Lewis, P., Lewis, S. L., Malhi, Y., Phillips, O. L., and Disney, M.: Assessment of bias in pan-tropical biomass predictions, Frontiers in Forests and Global Change, 3, 12, 10.3389/ffgc.2020.00012, 2020.

1835

1836

1837 Calders, K., Verbeeck, H., Burt, A., Origo, N., Nightingale, J., Malhi, Y., Wilkes, P., Raumonen, P., Bunce, R. G., and Disney, M.: Laser scanning reveals potential underestimation of biomass carbon in temperate forest, Ecological Solutions and Evidence, 3, e12197, 10.1002/2688-8319.12197, 2022.

1838

1839

1840 Chavana-Bryant, C., Wilkes, P., Yang, W., Burt, A., Bennett, A. C., Pickavance, G., Cooper, D., Lewis, S. L., Phillips, O. L., Brede, B., Herold, M., McNicol, I. M., Mitchard, E., Barbier, N., Vincent, G., Coomes, D. A., Jackson, T. D., Makaga, L., Milamizokou Napo, H. O., Ngomanda, A., Ntie, S., Medjibe, V., Dimbonda, P., Soenens, L., Daelemans, V., Bartholomeus, H., Majalap, N., Nilus, R., Labrière, N., Burslem, D. F. R. P., Qie, L., Derroire, G., Proux, L., Abernethy, K., Clewley, D., Moffat, D., Scipal, K., Vines, P., and Disney, M.: ForestScan: a multiscale dataset of tropical forest structure across 3 continents including terrestrial, UAV and airborne LiDAR and in-situ forest census data [dataset], 10.5285/88a0620229014e0ebacf0606b302112d, 2025.

1841

1842

1843

1844

1845

1846

1847 Chave, J., Réjou-Méchain, M., Bürquez, A., Chidumayo, E., Colgan, M. S., Delitti, W. B., Duque, A., Eid, T., Fearnside, P. M., and Goodman, R. C.: Improved allometric models to estimate the aboveground biomass of tropical trees, Global change biology, 20, 3177-3190, 10.1111/gcb.12629, 2014.

1848

1849

1850 Contributors, P.: PDAL VoxelCenterNearestNeighbor filter, PDAL documentation, available at: [code], 2025.

1851 Cuni-Sánchez, A., White, L. J., Calders, K., Jeffery, K. J., Abernethy, K., Burt, A., Disney, M., Gilpin, M., Gomez-Dans, J. L., and Lewis, S. L.: African savanna-forest boundary dynamics: a 20-year study, PLoS One, 11, e0156934, 10.1371/journal.pone.0156934, 2016.

1852

1853

1854 de Lima, R. A., Phillips, O. L., Duque, A., Tello, J. S., Davies, S. J., de Oliveira, A. A., Muller, S., Honorio Coronado, E. N.,  
1855 Vilanova, E., and Cuni-Sanchez, A.: Making forest data fair and open, *Nature Ecology & Evolution*, 6, 656-658,  
1856 10.1038/s41559-022-01738-7, 2022.

1857 Demol, M., Calders, K., Krishna Moorthy, S. M., Van den Bulcke, J., Verbeeck, H., and Gielen, B.: Consequences of vertical  
1858 basic wood density variation on the estimation of aboveground biomass with terrestrial laser scanning, *Trees*, 35, 671-684,  
1859 10.1007/s00468-020-02067-7, 2021.

1860 Demol, M., Aguilar-Amuchastegui, N., Bernotaite, G., Disney, M., Duncanson, L., Elmendorp, E., Espejo, A., Furey, A.,  
1861 Hancock, S., and Hansen, J.: Multi-scale lidar measurements suggest miombo woodlands contain substantially more carbon  
1862 than thought, *Communications Earth & Environment*, 5, 366, 10.1038/s43247-024-01448-x, 2024.

1863 Demol, M., Verbeeck, H., Gielen, B., Armston, J., Burt, A., Disney, M., Duncanson, L., Hackenberg, J., Kukenbrink, D., Lau,  
1864 A., Ploton, P., Sewdien, A., Stovall, A., Takoudjou, S. M., Volkova, L., Weston, C., Wortel, V., and Calders, K.: Estimating  
1865 forest above-ground biomass with terrestrial laser scanning: Current status and future directions, *Methods in Ecology and  
1866 Evolution*, 13, 1628-1639, 10.1111/2041-210x.13906, 2022.

1867 Derroire, G., Héault, B., Rossi, V., Blanc, L., Gourlet-Fleury, S., and Schmitt, L.: Paracou forest permanent plots (V3),  
1868 CIRAD Dataverse [dataset], 10.18167/DVN1/8G8AHY, 2023.

1869 Derroire, G., Héault, B., Rossi, V., Blanc, L., Gourlet-Fleury, S., and Schmitt, L.: ForestScan (DRAFT VERSION), CIRAD  
1870 Dataverse [dataset], doi/10.18167/DVN1/94XHID, 2025.

1871 Open3D library: [https://www.open3d.org/docs/0.9.0/tutorial/Basic/file\\_io.html#mesh](https://www.open3d.org/docs/0.9.0/tutorial/Basic/file_io.html#mesh), last access: November 2025.

1872 Duncanson, L., Armston, J., Disney, M., Avitabile, V., Barbier, N., Calders, K., Carter, S., Chave, J., Herold, M., and Crowther,  
1873 T. W.: The importance of consistent global forest aboveground biomass product validation, *Surveys in geophysics*, 40, 979-  
1874 999, 10.1007/s10712-019-09538-8, 2019.

1875 Duncanson, L., Kellner, J. R., Armston, J., Dubayah, R., Minor, D. M., Hancock, S., Healey, S. P., Patterson, P. L., Saarela,  
1876 S., and Marselis, S.: Aboveground biomass density models for NASA's Global Ecosystem Dynamics Investigation (GEDI)  
1877 lidar mission, *Remote Sensing of Environment*, 270, 112845, 10.1016/j.rse.2021.112845, 2022.

1878 Editorial: We must get a grip on forest science-before it's too late, *Nature*, 608, 449, 10.1038/d41586-022-02182-0, 2022.

1879 Fischer, F. J., Jackson, T., Vincent, G., and Jucker, T.: Robust characterisation of forest structure from airborne laser  
1880 scanning—A systematic assessment and sample workflow for ecologists, *Methods in ecology and evolution*, 15, 1873-1888,  
1881 10.1111/2041-210x.14416, 2024.

1882 ForestPlots.net, Blundo, C., Carilla, J., Grau, R., Malizia, A., Malizia, L., Osinaga-Acosta, O., Bird, M., Bradford, M.,  
1883 Catchpole, D., and Ford, A.: Taking the pulse of Earth's tropical forests using networks of highly distributed plots, *Biological  
1884 Conservation*, 260, 108849, 10.1016/j.biocon.2020.108849, 2021.

1885 RIEGL Laser Measurement Systems GmbH: <https://www.riegl.co.uk/>, last access: 01/01/2025.

1886 Goodman, R. C., Phillips, O. L., and Baker, T. R.: The importance of crown dimensions to improve tropical tree biomass  
1887 estimates, *Ecological Applications*, 24, 680-698, 10.1890/13-0070.1, 2014.

1888 Jackson, T. D., Fischer, F. J., Vincent, G., Gorgens, E. B., Keller, M., Chave, J., Jucker, T., and Coomes, D. A.: Tall Bornean  
1889 forests experience higher canopy disturbance rates than those in the eastern Amazon or Guiana shield, *Global Change Biology*,  
1890 30, e17493, 10.1111/gcb.17493, 2024.

1891 Jucker, T., Caspersen, J., Chave, J., Antin, C., Barbier, N., Bongers, F., Dalponte, M., van Ewijk, K. Y., Forrester, D. I., and  
1892 Haeni, M.: Allometric equations for integrating remote sensing imagery into forest monitoring programmes, *Global change  
1893 biology*, 23, 177-190, 10.1111/gcb.13388, 2017.

1894 Kellner, J. R., Armston, J., Birrer, M., Cushman, K., Duncanson, L., Eck, C., Falleger, C., Imbach, B., Král, K., and Krůček,  
1895 M.: New opportunities for forest remote sensing through ultra-high-density drone lidar, *Surveys in Geophysics*, 40, 959-977,  
1896 10.1007/s10712-019-09529-9, 2019.

1897 Krisanski, S., Taskhiri, M. S., Gonzalez Aracil, S., Herries, D., and Turner, P.: Sensor agnostic semantic segmentation of  
1898 structurally diverse and complex forest point clouds using deep learning, *Remote Sensing*, 13, 1413, 10.3390/rs13081413,  
1899 2021.

1900 Labrière, N., Davies, S. J., Disney, M. I., Duncanson, L. I., Herold, M., Lewis, S. L., Phillips, O. L., Quegan, S., Saatchi, S.  
1901 S., and Schepaschenko, D. G.: Toward a forest biomass reference measurement system for remote sensing applications, *Global  
1902 Change Biology*, 29, 827-840, 10.1111/gcb.16497, 2023.

1903 Lopez-Gonzalez, G., Lewis, S. L., Burkitt, M., and Phillips, O. L.: ForestPlots.net: a web application and research tool to  
1904 manage and analyse tropical forest plot data, *Journal of Vegetation Science*, 22, 610-613, 10.1111/j.1654-1103.2011.01312.x,  
1905 2011.

1906 Malhi, Y., Girardin, C., Metcalfe, D. B., Doughty, C. E., Aragão, L. E., Rifai, S. W., Oliveras, I., Shenkin, A., Aguirre-  
1907 Gutiérrez, J., and Dahlsjö, C. A.: The Global Ecosystems Monitoring network: Monitoring ecosystem productivity and carbon  
1908 cycling across the tropics, *Biological Conservation*, 253, 108889, 10.1016/j.biocon.2020.108889, 2021.

1909 Martin-Ducup, O., Mofack, G., Wang, D., Raumonen, P., Ploton, P., Sonké, B., Barbier, N., Couteron, P., and Pélassier, R.:  
1910 Evaluation of automated pipelines for tree and plot metric estimation from TLS data in tropical forest areas, *Annals of botany*,  
1911 128, 753-766, 10.1093/aob/mcab051, 2021.

1912 McNicol, I. M., Mitchard, E. T., Aquino, C., Burt, A., Carstairs, H., Dassi, C., Modinga Dikongo, A., and Disney, M. I.: To  
1913 what extent can UAV photogrammetry replicate UAV LiDAR to determine forest structure? A test in two contrasting tropical  
1914 forests, *Journal of Geophysical Research: Biogeosciences*, 126, e2021JG006586, 10.1029/2021JG006586, 2021.

1915 Momo, S. T., Ploton, P., Martin-Ducup, O., Lehnebach, R., Fortunel, C., Sagang, L. B. T., Boyemba, F., Couteron, P., Fayolle,  
1916 A., and Libalah, M.: Leveraging signatures of plant functional strategies in wood density profiles of African trees to correct  
1917 mass estimations from terrestrial laser data, *Scientific Reports*, 10, 2001, 10.1038/s41598-020-58733-w, 2020.

1918 Morhart, C., Schindler, Z., Frey, J., Sheppard, J. P., Calders, K., Disney, M., Morsdorf, F., Raumonen, P., and Seifert, T.:  
1919 Limitations of estimating branch volume from terrestrial laser scanning, *European Journal of Forest Research*, 143, 687-702,  
1920 10.1007/s10342-023-01651-z, 2024.

1921 Ochiai, O., Poulter, B., Seifert, F. M., Ward, S., Jarvis, I., Whitcraft, A., Sahajpal, R., Gilliams, S., Herold, M., and Carter, S.:  
1922 Towards a roadmap for space-based observations of the land sector for the UNFCCC global stocktake, *Iscience*, 26, 106489,  
1923 10.1016/j.isci.2023.106489, 2023.

1924 QGIS Geographic Information System: <https://qgis.org>, last access: November 2025.

1925 Quegan, S., Le Toan, T., Chave, J., Dall, J., Exbrayat, J.-F., Minh, D. H. T., Lomas, M., D'alessandro, M. M., Paillou, P., and  
1926 Papathanassiou, K.: The European Space Agency BIOMASS mission: Measuring forest above-ground biomass from space,  
1927 *Remote Sensing of Environment*, 227, 44-60, 10.1016/j.rse.2019.03.032, 2019.

1928 Ramachandran, N., Saatchi, S., Tebaldini, S., d'Alessandro, M. M., and Dikshit, O.: Mapping tropical forest aboveground  
1929 biomass using airborne SAR tomography, *Scientific Reports*, 13, 6233, 10.1038/s41598-023-33311-y, 2023.

1930 Raumonen, P., Kaasalainen, M., Åkerblom, M., Kaasalainen, S., Kaartinen, H., Vastaranta, M., Holopainen, M., Disney, M.,  
1931 and Lewis, P.: Fast automatic precision tree models from terrestrial laser scanner data, *Remote Sensing*, 5, 491-520,  
1932 10.3390/rs5020491, 2013.

1933 Roussel, J.-R., Auty, D., Coops, N. C., Tompalski, P., Goodbody, T. R. H., Sánchez Meador, A., Bourdon, J.-F., de Boissieu,  
1934 F., and Achim, A.: lidR: An R package for analysis of Airborne Laser Scanning (ALS) data, *Remote Sensing of Environment*,  
1935 251, 112061, <https://doi.org/10.1016/j.rse.2020.112061>, 2020.

1936 Saatchi, S., Chave, J., Labrière, N., Barbier, N., Réjou-Méchain, M., Ferraz, A., and Tao, S.: AfriSAR: Aboveground Biomass  
1937 for Lope, Mabounie, Mondah, and Rabi Sites, Gabon [dataset], 10.3334/ORNLDaac/1681, 2019.

1938 Saatchi, S. S., Harris, N. L., Brown, S., Lefsky, M., Mitchard, E. T., Salas, W., Zutta, B. R., Buermann, W., Lewis, S. L., and  
1939 Hagen, S.: Benchmark map of forest carbon stocks in tropical regions across three continents, *Proceedings of the national  
1940 academy of sciences*, 108, 9899-9904, 10.1073/pnas.1019576108, 2011.

1941 Sabah Forestry Department: Official Website: <https://forest.sabah.gov.my/>, last access: 14/01/2025.

1942 Schepaschenko, D., Chave, J., Phillips, O. L., Lewis, S. L., Davies, S. J., Réjou-Méchain, M., Sist, P., Scipal, K., Perger, C.,  
1943 and Herault, B.: The Forest Observation System, building a global reference dataset for remote sensing of forest biomass,  
1944 *Scientific data*, 6, 198, 10.1038/s41597-019-0196-1, 2019.

1945 CloudCompare (3D point cloud and mesh processing software) version 2.13: <https://www.cloudcompare.org>, last access:  
1946 November 2025.

1947 Verhelst, T. E., Calders, K., Burt, A., Demol, M., D'hont, B., Nightingale, J., Terryn, L., and Verbeeck, H.: Implications of  
1948 Pulse Frequency in Terrestrial Laser Scanning on Forest Point Cloud Quality and Individual Tree Structural Metrics, *Remote  
1949 Sensing*, 16, 4560, 10.3390/rs16234560, 2024.

1950 Vincent, G., Verley, P., Brede, B., Delaitre, G., Maurent, E., Ball, J., Clocher, I., and Barbier, N.: Multi-sensor airborne lidar  
1951 requires intercalibration for consistent estimation of light attenuation and plant area density, *Remote Sensing of Environment*,  
1952 286, 113442, 10.1016/j.rse.2022.113442, 2023.

1953 White, L., Rogers, M. E., Tutin, C. E., Williamson, E. A., and Fernandez, M.: Herbaceous vegetation in different forest types  
1954 in the Lopé Reserve, Gabon: implications for keystone food availability, *African Journal of Ecology*, 33, 124-141,  
1955 10.1111/j.1365-2028.1995.tb00788.x, 1995.

1956 Wilkes, P. and Yang, W.: rxp-pipeline: Tools to transform RIEGL terrestrial LiDAR, Zenodo [code], 2025a.

1957 Wilkes, P. and Yang, W.: mat2ply: Tools for converting QSM data to 3D PLY models., Zenodo [code], 2025b.

1958 Wilkes, P., Krisanski, S., Clewley, D., Moffat, D., and Yang, W.: TLS2trees (Version 0.1) Zenodo [code], 2025.

1959 Wilkes, P., Lau, A., Disney, M., Calders, K., Burt, A., de Tanago, J. G., Bartholomeus, H., Brede, B., and Herold, M.: Data  
1960 acquisition considerations for terrestrial laser scanning of forest plots, *Remote Sensing of Environment*, 196, 140-153,  
1961 10.1016/j.rse.2017.04.030, 2017.

1962 Wilkes, P., Disney, M., Armston, J., Bartholomeus, H., Bentley, L., Brede, B., Burt, A., Calders, K., Chavana-Bryant, C.,  
1963 Clewley, D., Duncanson, L., Forbes, B., Krisanski, S., Malhi, Y., Moffat, D., Origo, N., Shenkin, A., and Yang, W. X.:  
1964 TLS2trees: A scalable tree segmentation pipeline for TLS data, *Methods in Ecology and Evolution*, 14, 3083-3099,  
1965 10.1111/2041-210x.14233, 2023.

1966 Zanne, A. E., Lopez-Gonzalez, G., Coomes, D. A., Ilic, J., Jansen, S., Lewis, S. L., Miller, R. B., Swenson, N. G., Wiemann,  
1967 M. C., and Chave, J.: Global wood density database [dataset], 10.5061/dryad.234, 2009.

1968